ENHANCED SINTERING OF YSZ CERAMICS WITH LOW LEVEL NICKEL OXIDE DOPANTS

by

Zane Douglas Townsend

A thesis is submitted in partial fulfillment
of the requirements for the degree

of

Master of Science

In

Mechanical Engineering

Montana State University
Bozeman, MT

May 2009

APPROVAL

of a thesis submitted by

Zane Douglas Townsend

This thesis has been read by each member of the thesis committee and has been found to be satisfactory regarding content, English usage, format, citation, bibliographic style, and consistency, and is ready for submission to the Division of Graduate Education.

Stephen W. Sofie, PH.D.

Approved for the Department of Mechanical Engineering

Christopher H. M. Jenkins, PH.D., P.E.

Approved for the Division of Graduate Education

Dr. Carl A. Fox

STATEMENT OF PERMISSION TO USE

In presenting this thesis in partial fulfillment of the requirements for a master's degree at Montana State University, I agree that the Library shall make it available to borrowers under rules of the Library.

If I have indicated my intention to copyright this thesis by including a copyright notice page, copying is allowable only for scholarly purposes, consistent with "fair use" as prescribed in the U.S. Copyright Law. Requests for permission for extended quotation from or reproduction of this thesis in whole or in parts may be granted only by the copyright holder.

Zane Douglas Townsend

May 2009

ACKNOWLEDGEMENTS

I would like to express profound gratitude to my advisor, Dr. Stephen Sofie, for his invaluable support, encouragement, supervision and useful suggestions throughout my research. His enthusiasm and extensive knowledge base proved to be an invaluable motivation. I would also like to thank Dr. Vic Cundy and Dr. David Miller for their support as committee members. My gratitude goes out to Dr. Ahsan Mian and C-L Tsai for the use of their labs for this research, as well as all of the members of Dr. Sofie's Lab who helped in many ways with my research: Max Lifson, Melissa Donaldson, John McCrummen, and Paul Gentile.

Deep appreciation goes to my fellow graduate students as well as the entire staff of the Mechanical and Industrial Engineering Department. Special thanks go to my parents Mark and Leslie Townsend for their continuous support and motivation through my college career. I would like to thank Barbara Martin for helping me maintain focus during the times of increased stress.

TABLE OF CONTENTS

TABLE OF CONTENTS CONTINUED

TABLE OF CONTENTS CONTINUED

LIST OF TABLES

LIST OF FIGURES

Figure Page

LIST OF FIGURES CONTINUED

Figure Page

LIST OF FIGURES CONTINUED

Figure Page

LIST OF FIGURES CONTINUED

Figure Page

LIST OF EQUATIONS

ABSTRACT

Tape casting is an effective method for obtaining thin YSZ electrolytes used in solid oxide fuel cells. While the costs of YSZ have decreased from demand and improved manufacturing, large amounts of energy are required to properly densify the ceramic material inflating of the overall cost of this material. YSZ must be completely dense to ensure that the fuels used for power generation do not combine resulting in failure of the cell. The purpose of this research is to determine the effectiveness of low level nickel oxide dopants as a sintering aid to reduce the high sintering temperature process while also evaluating the mechanical and ionic conduction behavior.

Baseline samples, of both 8YSZ and 3YSZ, were tested and compared to samples doped with concentrations of nickel oxide up to 1 mole %. Transition metal additives may have the potential to increase the electrical conductivity and/or decrease the ionic conductivity of the YSZ, therefore only a maximum of 1 mole % nickel was added to the ceramic powder. It was determined that one mole percent of nickel oxide added to the traditional tape casting slurry achieved the greatest improvement in theoretical density, sintering rate, and onset of densification at 1300°C using standard micron sized powders. Utilizing impedance spectroscopy, it was shown that overall the nickel dopant yielded a negligible change in total conductivity, however, it is noted that a slight increase in the grain boundary contribution was observed for the doped specimens. Mechanical strength testing was conducted with a concentric ring on ring compressive flexural strength standard according to ASTM guidelines indicating an average 40% increase in strength over the undoped specimens for all sintering temperatures. Evaluation of grain size and fracture patterns for doped and undoped specimens indicates significant grain growth and a transition to transgranular fracture with the doped specimens.

INTRODUCTION

Fabricating solid oxide fuel cells that are less expensive and effective for timely commercialization is a vital component in the implementation of alternative energy systems. The core of the solid oxide fuel cell, the electrolyte, is a primary target for achieving additional cost reductions. Traditional tape casting of solid oxide fuel cell electrolytes is a common practice for preparing large area thin substrates. While this process has been well establish for commercial use for fabricating customized electrolytes to meet specific application requirements, tape cast YSZ often requires sintering temperatures from 1400 – 1500°C to achieve non-porous, high strength components (1). In this manner, a key means to drive down the cost of the SOFC manufactures is to lower the sintering temperature of the electrolyte. This temperature reduction serves two purposes by first reducing the energy costs associated with high temperature sintering in addition to facilitating co-sintering approaches that reduce cost by limited the number of manufacturing steps.

Co-sintering is the process in which the electrodes and the electrolyte can be sintered simultaneously producing porous structure for the electrodes and a hermetic membrane from the electrolyte. This eliminates the need for a multi-stage process to produce a single cell. An important limitation to the broad use of co-sintering is the sensitivity of the YSZ electrolyte and lanthanum strontium magnate cathode material. At temperatures above 1300°C a secondary zirconate phase forms thus inhibiting both ionic and electrical conduction at the interface, substantially effecting performance and durability of the cell. (2; 3)

The addition of small amounts of transition metal oxides (nickel oxide) into the tape slurry is being evaluated in this study to reduce the sintering temperature of YSZ to the 1300°C threshold to inhibit deleterious phase formation. The use of nickel oxide as an electrolyte dopant has several key benefits in that the raw material is inexpensive and it is heavily used in SOFC anode preparation, thus readily available for electrolyte processing. While improved densification and strength are primary outcomes of the study, an additional focus of this study is to also evaluate the ionic conduction behavior of YSZ with metal oxide dopant, as the benefits of sintering could easily be abated if the nickel oxide degrades the ionic conductivity.

BACKGROUND

Overview of Fuel Cell

In order to understand the critical part that the electrolyte plays in the operation of a solid oxide fuel cell the fundamentals of operation must be understood. Fuel cells are used to create electricity from a chemical fuel, however, unlike a combustion process, the fuel cells have no moving parts. They have a high efficiency, low emission, and low noise pollution. Their efficiency is remarkably higher than traditional power generation methods because fuel cells are not limited by the Carnot efficiency and do not rely on moving parts to create useable power. No frictional losses occur during power generation in the solid state electrochemical process. The electrochemical conversion is a continuous catalytic process. (4)

The components of a fuel cell are an anode, cathode, and electrolyte; together they are referred to as the membrane-electrode assembly (MEA). The MEA, also called a single cell fuel cell, is shown in Figure 1. The anode and cathode are the electrodes that sandwich the electrolyte. These are porous to let the gasses infiltrate while the electrolyte is manufactured to be dense to prevent the fuels from mixing (5). The Nernst potential is only possible with a dense electrolyte which causes a large concentration gradient of oxygen that drives the electrochemical process. A high concentration gradient across the ion permeable membrane results in higher power generation from the single fuel cell. (6)

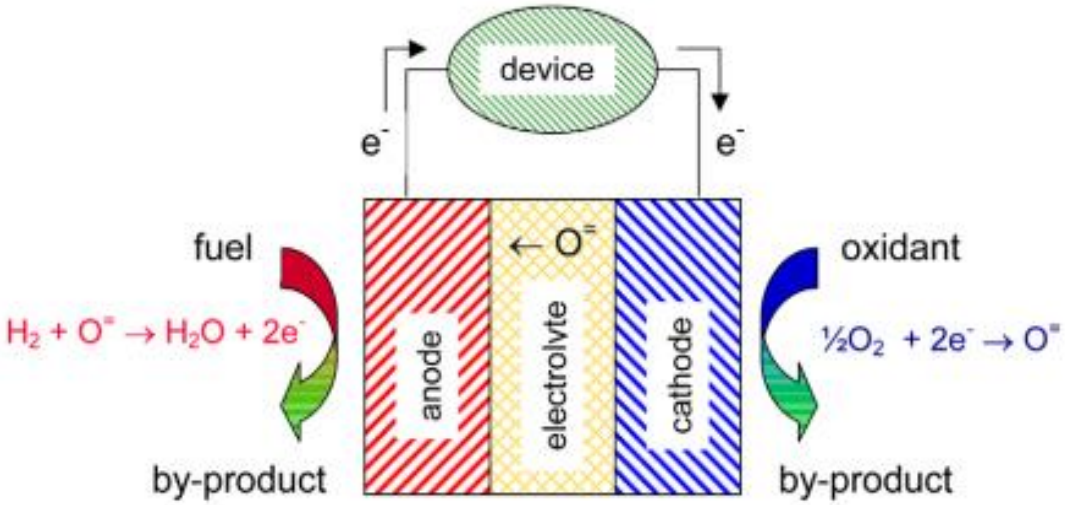

Figure 1. Single Cell Fuel Cell Configuration (5)

In a solid oxide fuel cell (SOFC) the hydrogen is introduced on the anode side while oxygen is introduced on the cathode side. The electrolyte is an ionic conductor permitting the oxygen ions to diffuse through the electrolyte membrane from the cathode to the anode side. An oxygen pressure gradient is the driving force behind the diffusion through the electrolyte from the air to the fuel side. The anode/electrolyte interface is the location in the fuel cell where heat and water are formed, also known as the triple phase boundary (TPB) as shown in Figure 2. This is where gas in oxidized in the electrochemically active region which is a three phase boundary of an ionic conducting phase (YSZ), electronically conducting phase (Ni), and gas phase of H_2 and $C_{O.}$

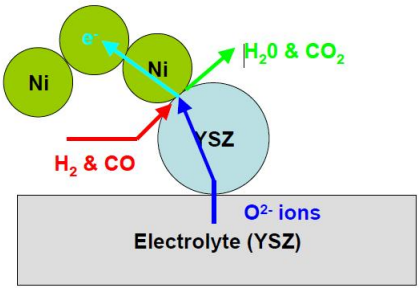

Figure 2. Triple Phase Boundary Region

Electrons are formed at the layer between the electrolyte and the cathode, combine with 0_2 atoms and are transported through the electrolyte as shown in Figure 3. The circuit is completed at the anode, providing electrical energy to the external circuit. When combined at the anode TPB, the oxygen ions react with the hydrogen ions producing water as the waste product releasing electrons. Ion conduction is a thermally driven process so the material and temperature used in the process are the large contributing factors for efficiency. (5; 7)

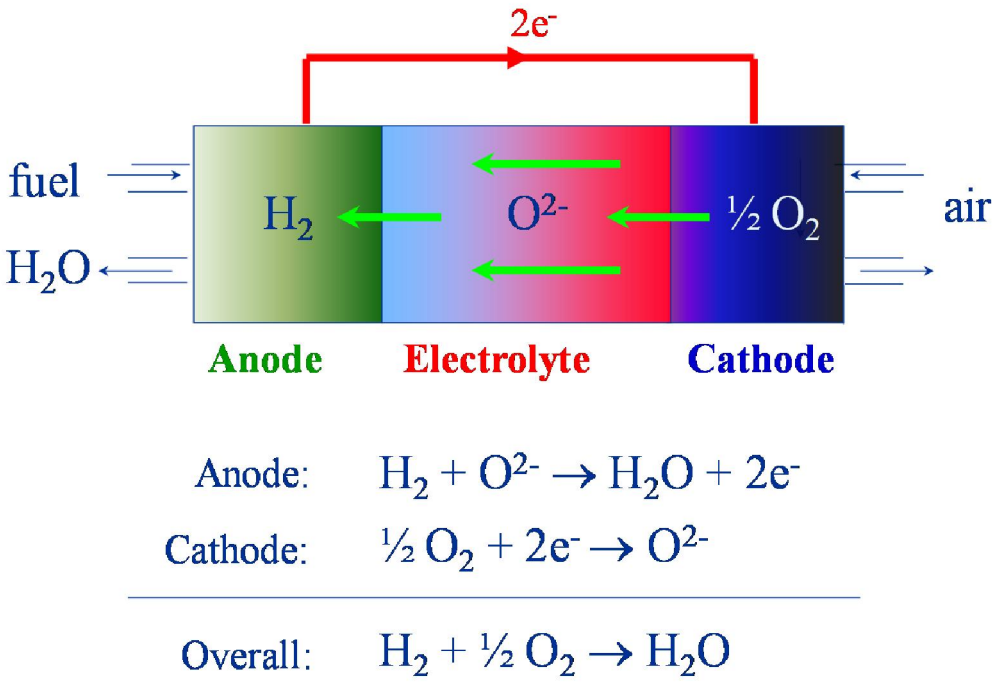

Figure 3. Overall Reaction of Hydrogen and Oxygen In A Single Cell Fuel Cell (8)

The triple phase boundary is the region where the electrochemical reactions take place. This region is where the anode interacts with the electrolyte. The area becomes engaged when it has electrical contact with the electrode, is exposed to the reactant, contains sufficient electro-catalyst for the reaction to progress at an optimum rate, and in ionic contact with the electrolyte. (9)

SOFC Fuel Cell Components

The single cell fuel cell is made up of three individual components to produce energy. The three separate components must have unique material qualities to produce a working fuel cell. High temperature, chemical reactions, and structural stability are all factors when designing the MEA. The thermal expansion of the three components must be similar to each other to minimize thermal stresses during the thermal cycling. This helps prevent mechanical failure of any individual mechanism.

Cathode

A cathode must be porous to allow the oxygen to reach the electrolyte/cathode interface. Cathode material is most commonly lanthanum manganite ($LaMnO_3$) doped with strontium to create LSM ($La_{1-x}Sr_xMnO_3$) (5). While cobalt and iron based compounds are also being evaluated such as lanthanum ferrite doped with strontium (LSF), and lanthanum chromite doped with strontium (LSC), and lanthanum cobalt iron oxide doped with strontium (LSFC), LSM has demonstrated the highest levels of stability for commercial applications (10; 11). Strontium is used to increase the electrical conductivity of the cathode material. LSM proves to be harmonious with yttria-stabilized zirconia (YSZ) which is the most common material used for electrolytes. Beyond 1300ºC these materials react and form an insulating layer (2; 3; 1). This is the secondary driver for the doping strategies, to inhibit this phase formation with lower temperature processing.

Electrolyte

The electrolyte membrane must be moderately dense, greater than approximately 93% theoretical to eliminate open porosity, to prevent short circuiting caused by the gasses flowing through it. The electrolyte should also be as thin and strong as possible to ensure structural integrity and minimize the resistive losses (12). Membranes in SOFCs, must provide high ionic conductivity under high operating temperatures, however, electrical conductivity cannot be present for ion migration to occur. Electrical conductivity would disrupt the chemical reaction (13). A field proven material used for the electrolyte is YSZ due to the characteristics it maintains at high temperatures around 800ºC. The stability of the zirconia-based electrolyte is well established, however ceria-based electrolytes have notable advantages. Higher conductivities are achieved at lower operation temperatures, and they demonstrate a strong relation with high performance cathode material. (5; 13; 14).

While YSZ has many applications focus in solid oxide fuel cells and automotive oxygen sensors, YSZ is also a prominent material in the development of bio-implants, computer displays, automotive sensors, and thermal plasma sprays for aerospace use (15; 16). Beyond improving the processing of solid oxide fuel cells, the addition of nickel dopant or other transition metal dopants could enhance the sintering performance, as well as the mechanical properties for these applications.

Anode

The anode is very similar to the cathode as it must be porous and have a high electrical conductivity, but also must function in a reducing atmosphere. Nickel doped yttria-stabilized zirconia is a common material of choice for the anode material in SOFCs. Nickel is inexpensive and is nearly as effective of a hydrogen oxidation catalyst as platinum at high temperature. The Ni-YSZ produces a porous structure and nickel proves to be one of the most abundant and affordable metals. (7; 5; 13)

Pore formers such as starch are used to help create the pores for gas transport and are burned out during the sintering process. YSZ is used in the anode, to extend the triple phase boundary beyond a planar interface, as shown in Figure 2. The extension of the (TPB) improves the cell performance. (5; 7; 17)

Interconnects

The interconnects are the devices that allow the fuels to reach the anode and cathode, collect the energy, and keep the fuel and oxidant separate in the system. Interconnects are placed in between the individual single cell fuel cells to create a stack of cells. The stack shown in Figure 4 allows the cells to create enough power for general use. The design of an interconnect must take into account many constraints. Operating temperature of a solid oxide fuel cell is in the range of 800-1000° Celsius. The atmospheres of the cathode and anode cannot mix, therefore the interconnect must not be porous. The MEA must have a close thermal expansion to that of the interconnect to keep thermally induced internal stresses to a minimum. (7)

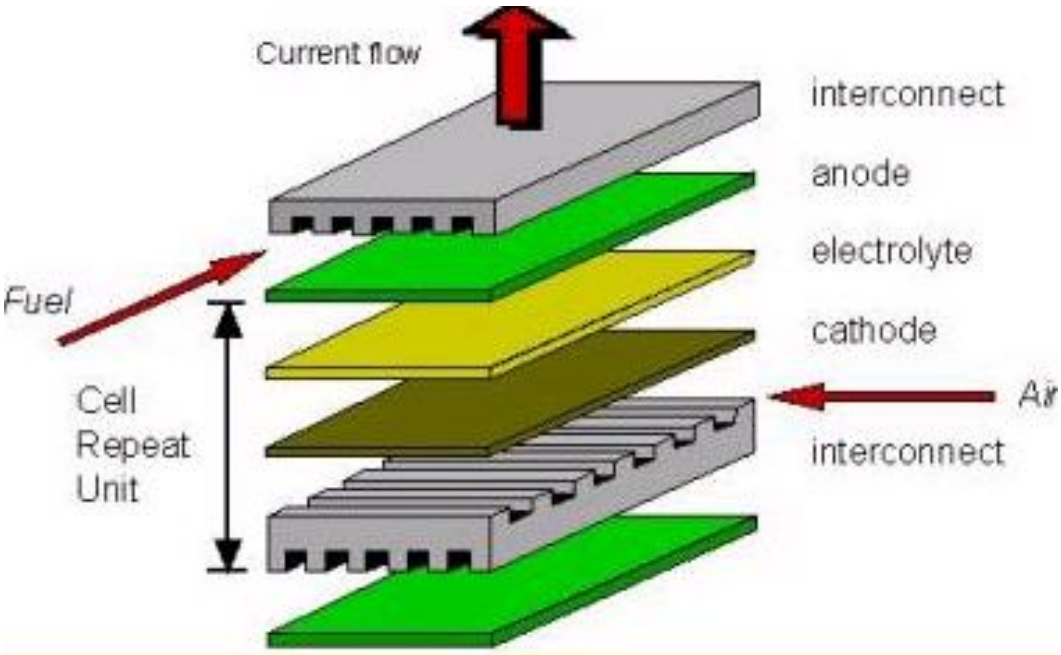

Figure 4. Fuel Cell Stack (7)

The energy that is produced by a single cell is minimal. Therefore, a stack of cells is coupled with interconnects in series to achieve a useable level of energy. A single cell operating under a load generates about 0.7V at a maximum power density and approximately 1.2V in an open circuit. (4)

The process ideally could run as long as fuel is supplied to the system. The fuel used for power generation can vary greatly. Hydrogen and carbon monoxide can be used with the use of a fuel reformer. These are in the form of syngas from any hydrocarbon fuel such as methanol, gasoline, diesel, methane, and natural gas. (14)

SOLID OXIDE FUEL CELL MANUFACTUREING

To combine all the components that make up the single cell fuel cell is a tedious task; it can be difficult to repeat and is a delicate procedure. The lowering of the sintering temperature of the electrolyte would make it possible to sinter all the components simultaneously, reducing manufacturing time and cost.

Characteristics of the electrolyte, as discussed earlier, must be completely dense while the electrode components must be porous for gas transfer. This could feasibly be obtained at the same time during one sintering cycle. Post sintering is the current practice of making SOFCs; each individual part is sintered at different temperatures and times. The electrolyte is sintered first at a high temperature to achieve the proper densification. Cathode electrode material is then applied to the electrolyte and the two components are then sintered at a slightly lower temperature. In the last step the anode material is applied on the side opposite from the cathode and the entire MEA is sintered a third time at a lower temperature than previously sintered. Post sintering takes three times longer than co-sintering due to different temperatures being used at each step of the manufacturing process. Nickel dopant has the potential to make co-sintering a viable option for SOFC manufacturing.

SOFC TECHNOLOGICAL MERIT

Fuel cells contain no moving mechanical parts, eliminating the noise and vibration experienced during conventional electric generators. If hydrogen is the fuel utilized for power generation the main by-product of the chemical reaction is water. The solid oxide variety of fuel cells can be placed in remote areas easily and can be used with a wide range of fuels (5).

Electrolytes can be manufactured according to a specific shape, such as tubular or planar. These types are shown in Figure 5. The three phase boundary region can be tailored based on desired fuel conversion rate and power generation. The tubular configuration ideal for stationary power generation has cold seals and a low power density. The planar design has hot seals with a high power density which is ideal for mobile use. (18; 19; 20)

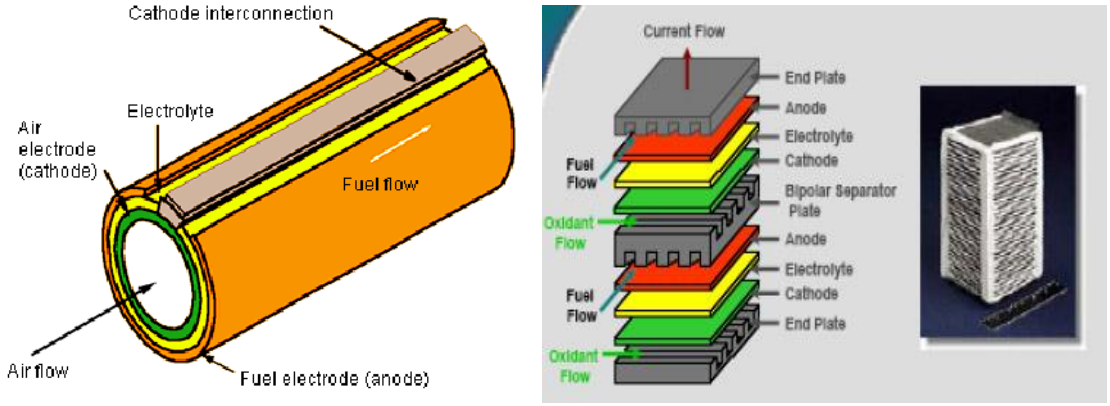

Figure 5. Tubular (Left) (21) and Planar (Right) SOFC Design (22).

The raw efficiency of a SOFC is in the range of 40-60% while traditional chemical combustion systems yield substantially lower efficiencies. Furthermore, a

hybrid system consisting of a gas turbine and an SOFC has an efficiency of 70% or higher as displayed in Figure 6 (5). A hybrid system shown in Figure 7 combines an SOFC with a gas turbine to reach high levels of efficiency. The entire system is under pressure, increasing the SOFC performance alone. Hot exhaust from the fuel cell becomes a pressurized gas flow that can operate the gas turbine (23; 24). The exhaust could also be used to operate thermoelectric systems, or be used for combined heat and power (CHP). (25)

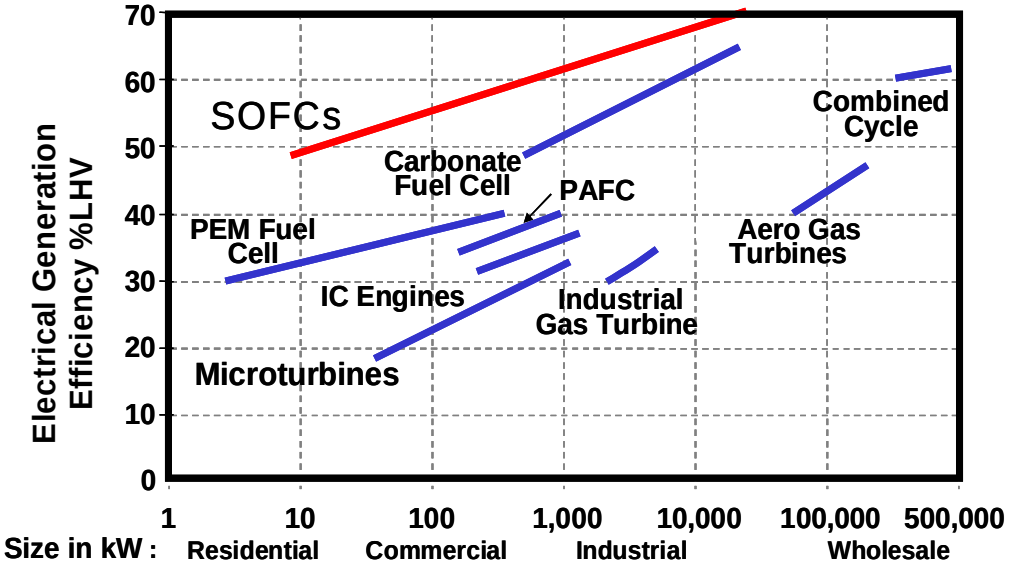

Figure 6. Electrical Efficiency vs. Size (19)

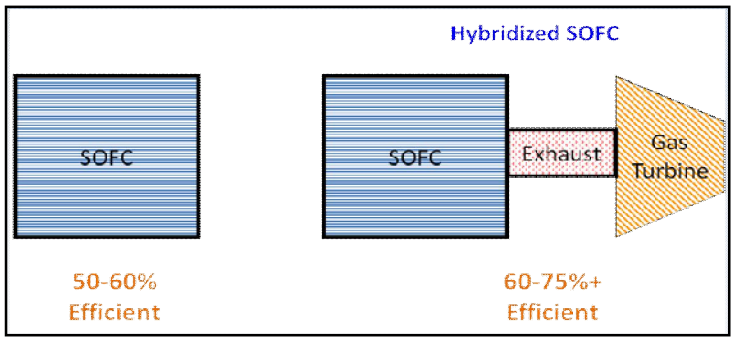

Figure 7. Hybrid SOFC System (26)

The high manufacturing cost of solid oxide fuel cells can slow the commercialization of the cells. The technical maturity of SOFCs are lower than other current power generating systems limiting the immediate implementation. Further, SOFCs do not perform with intermittent use; the start up time can be a lengthy process. The entire system must reach the high operating temperature without damaging the internal parts from mismatched CTE. SOFCs are inherently fuel flexible with the least reactive of the fuels that can be used for power generation need to be run through a reformer to achieve the hydrogen and oxygen levels required for the chemical process. However, the reformer is internal in SOFCs but sulfur removal must be done prior to the fuel being used. High operating temperature requires the sealing of planar stacks to use hot seals. However, the high operating temperature is beneficial to hybridization, sulfur tolerance, and allows the use of nickel instead of noble metals in SOFCs (23; 25; 24; 27). Lowering the temperature at which a fuel cell can operate is desirable for mobile and quick start applications; however, the electrode activity becomes less than optimum with decreasing temperature (7; 24). Research is continuing to try to solve the inherent problems with the manufacturing, operation, and longevity of SOFCs.

SOFC Applications

There are three main focuses for solid oxide fuel cells. These areas are military application, stationary power, and limited transportation. The appeal for the military is the necessity of remote power generation. SOFCs will produce power with little preparation and produce no noise at low pollution levels with minimal environmental

impact. "Moreover, the use of fuel cells could significantly reduce deployment cost: 70% by weight of the material that the military moves is nothing but fuel (5)."

Stationary power generation could be established in remote areas for endless application use where a fuel source is available (24). Already, working models have gone through hundreds of thermal cycles and years of operation with minimal losses (5; 28). Stationary power is the focus for solid oxide fuel cells as well as providing a feasible power generation alternative for either main or backup power.

Transportation is another area of interest with alternative energy. Personal cars are numbered in the millions. With the environmental issues and climbing fuel prices, alternative power generation is becoming very attractive. SOFCs could help lead the way to personal transportation with minimal pollution while also using inexpensive fuels. Trucks and buses could also implement solid oxide fuel cell use. The power generated from an SOFC could be used for lights and other electrical devices such as air conditioning (5; 20). The reduction on the power generation would use less fuel reducing cost in transportation.

SOFCs can also be used as reactors for synthesis of hydrogen and carbon monoxide by partially oxidizing hydrocarbons or reforming steam. Hydrogen rich gas and electricity can be generated collectively when reforming hydrocarbons with an SOFC (29). This application of SOFCs could aid in the construction of hydrogen infrastructure in the country and could be placed in remote locations where hydrocarbons are currently in use.

ADVANCED CERAMICS

It is quite common for ceramic materials to be engineered for specific applications. Some examples of ceramic uses include glass, abrasives, space shuttle tiles, magnets, joint replacements, and superconductors (30). Ceramics can be used in almost any field and new discoveries are made constantly. However, their properties and limitations must be taken into account when designing and working with them.

Structural

Oxide ceramics are an important class of materials involving the combination of oxygen with typical transition and rare earth metals. Alumina, alumina silicate, zirconia, and silica are all oxide ceramics. The low degradation of strength and modulus at high temperatures makes ceramics the most effective solution over metal at extreme temperatures and environments particularly for wear and thermal protection applications. The inherently low fracture toughness of oxides limits their use in applications requires tensile loading given the propensity for catastrophic fast fracture. (31; 32; 33)

The replacement of metal with oxygen usually results in a decrease in density which can be a benefit for light weighting technology particularly those pertinent to aerospace development. The modulus of rupture of ceramics is highly dependent on flaws within the brittle material. Larger density inherently increases the modulus of rupture of breaking strength of the ceramic by decreasing internal flaws. Less dense porous ceramics contain many internal pores which provide a thermal barrier, and can improve the toughness which is basis of high performance insulations. (31; 32)

Functional

While oxides cannot readily meet the mechanical requirements for metals in structure designs, oxides have unique electronic and optical properties that stand apart from metallic materials. These so called function properties are the key factors that drive alternative energy development as well as sensors, actuators, and filtration membranes (34; 35). There functional properties are embodied in electrical conduction, ionic conduction, thermal conduction that is decoupled from electronic conduction, high melting temperature, stability in oxidizing environments, and wear resistance (31; 33).

CERAMIC PROPERTIES

Ceramic properties are often compared with metal properties, such as modulus of elasticity, toughness, and strength. The reason for the comparison is metals have a large database with experimental results which then ceramics can be evaluated to. Ceramics do have some different properties than metals due to the different material structure (36). Ceramics have the ability to prevent electrical and thermal conduction at high temperature. The opposite is true for metallic material due to the freedom of the valance electrons (free electrons). The free electrons permit the flow electrons transporting heat and electricity. The electrons are free to flow and carry a charge for electrical conduction. Elevated temperatures cause the electrons to be more active from kinetic energy resulting in high thermal conduction (32; 33; 36). In environments with extreme thermal and chemical conditions, ceramics are more stable than metals.

The structure of ceramics inherently makes ceramics stronger in compression than tension due to the inherent brittleness. Ceramics fail suddenly in tension while Metals are comparable in tensile and compressive strength (32; 36). The limitations of ceramics must be considered in a design process, yet the versatility of the material makes it vital for many applications dealing with heat and temperature such as solid oxide fuel cells.

Elastic Properties

Ceramics inherently have a higher modulus of elasticity than other materials due to the strength of the interatomic bonds of the material. The two bonds associated with

ceramics are ionic and covalent which have high stiffness due to the position sensitivity and directionality (36; 33; 32). The modulus of elasticity is the value of the amount of stress used to produce a single unit of elastic strain (37). Elastic strain comes from a material that has a minimal stress applied, or for a short time span; the strain that is induced will disappear when the applied stress is released. Stress that is applied excessively will break down the atomic spacing and will result in plastic deformation. The modulus of elasticity is also dependent on the temperature of the material. Higher temperatures result in a higher level of material compliance. The higher the temperature of a material the lower the modulus of elasticity becomes (37).

Thermal Conductivity

Ceramics have a notable difference from metals when dealing with thermal energy. Traditional metals have higher thermal conductivity than ceramics. The amount of free electrons plays a critical role in the thermal conductivity of a material; the more electrons available, the more energy that can be transferred. Ceramics have few free electrons, creating very little energy per unit volume, low velocity, and short mean free path (36). Ceramic semiconductors have a slightly higher number of free electrons than general ceramic materials. Semiconductors need to reach high temperatures to conduct significant amounts of heat (32). Ceramics have great ionic and covalent bonding with few free electrons which makes them perfect for high temperature applications.

The Lorentz number is the ratio of the thermal conductivity to the product of electrical conductivity and temperature (38). For most metals the number is

approximately constant due to the driving force of free electrons for both properties independent of temperature (39). However, the Lorentz number is not constant for ceramics due to the lack of electrical conductivity even when high levels of thermal conduction is present from lattice vibration (40).

Electrical Conductivity

Similar to thermal conductivity, electrical conductivity is highly dependent on the free electron count. With minimal free electrons associated with ceramics, the electrical conductivity of the material goes down. Electrical conductivity is the capability of a material to transmit the flow of electrons (36). The internal structure of ceramics also limits the charge transfer by restricting the movement of electrons. Ceramics do not have many free electrons. Free electrons are the loosely attached electrons that are the furthest away from an atoms nucleus. The more free electrons available the higher the electrical conductivity is for that certain material. Thermal activity will raise the electrical conductivity in materials by forcing more electron movement. (32; 36)

The more defects there are in a material, the higher the chance of it becoming more electrical conductive. The extra space produced from the defect allows for the electrons to start unrestricted movement (32; 41). The properties of ceramics highlight the qualities sought after for the use and development of new technologies in solid oxide fuel cells.

PROCESSING

Achieving dense ceramic parts with the properties and characteristics described previously starting with fine powders requires intermediate processes to achieve sizes and shapes needed for the end product. The desired process for this research was to manufacture constant, thin ceramics which can be duplicated. Tape casting was used to create the thin tapes of ceramics from an organic based mixture, also known as slurry. The main ingredients in the slurry are solvents, surfactants, binders, plasticizers, and ceramic powder. The powder selection for the manufacturing process is the first ingredient to consider. Binders are then chosen based on the powder followed by a solvent to dissolve the ingredients (42). The slurry is processed by tape casting to acquire the desirable solid state shapes, as described in the tape casting section. The sintering process is the final step which forms the ceramic into a desired end product that can be used in specific applications. During the firing process the residual ingredients are burned out and the ceramic power particles are left, thermally and chemically joined (43).

Ceramic Powders

The ingredient left after all the processing is the powder, making it the most vital ingredient in the batch. All the other components of the batch are simply for the fabrication and desired product qualities. The powders used contain many important aspects that cannot be overlooked. Particle size and distribution play a key role in what type of ingredients to use, as well as the quantity required for the tape recipe (44). The distribution and size of particles account for the density of the tape prior to sintering

(green tape) in a tape casting process. Tape casting also allows for the tape to shrink, producing dense tapes prior to sintering. The surface area of the ceramic particles must have an average size, for coating consistency, and the impurities in the powder should be minimal. Slight variation in particle size can be advantageous. Smaller particles will fill the voids created by larger particles, enhancing the packing density (44). An average surface area will let the dispersant homogenize the slurry for repeatable batch results (42). The most common powder for electrolyte use in SOFCs, is yttria-stabilized zirconia (YSZ). The cathode powder used most often is lanthanum manganese oxide doped with strontium (LSM). Particle sizes that are commonly dealt with in ceramic processing are microscale and nanoscale.

Solvents

A solvent must be used to make a fluid forming process. It is used to make a homogenous mixture by dissolving all of the components of the slurry. The solvent is a fluid with a viscosity that allows the ceramic powder to be formed into a uniform sheet. Tape casting is conducted mainly with non-aqueous solvents for improved drying time. The standard organic solvents used for casting consist of ethanol, methanol, xylenes, and toluene (42).

Water based or organic based solvents are commonly used for traditional ceramic processing. The setback when dealing with a water-based tape is the inability to dissolve the binders and achieve high packing order of the particles. Organic based solvents not only dissolve the constituents in the slurry more efficiently but increases the drying time

of the processed ceramic. The common practice is to use binary or two solvents, in a tape. Using two solvents will help increase the ability to dissolve the ceramic powder, increase drying time, and reduce cost (45). The solvents that are chosen for the tape will determine the other ingredients and can be specifically tailored to a certain process (42). The tape cast will not be optimal if the solvent does not work correctly. All of the ingredients must be dissolved completely while suspending the powder evenly with no adverse effects.

Surfactants

A surfactant, or surface active agent, modifies the surface of a particle. Surfactants are vital to dispersion, wetting, high density, porosity, and green strength. Once the powder is mixed with the solvents the dispersant is added. The dispersant is used to separate and hold the particles for coating. The solids loading increases with the addition of dispersants to ensure powder suspension and facilitate faster drying with minimal shrinkage (42).

Van der Waals forces are the forces that attract and bind particles electrostatically. The forces must be overcome to insure a tape that is of desired quality. Clumps of particles will form if the attractive forces are not broken by the dispersion materials (46). A tape that has a suspension of fluid with properly dispersed particles has a low viscosity. The low viscosity is a function of the particle mobility caused by the fluid inter-particulate layer. The suspension of well dispersed particles is the key to achieving dense

ceramic tapes (42). Denser green tapes help to alleviate air bubbles and other imperfections from affecting the ceramic during firing.

Binders

Binders are a very important ingredient in the slurry. They are the only continuous phase in the green state and therefore control various tape properties such as flexibility, strength, and smoothness. Binders enable the green tape to be handled and prepared for sintering without causing damage to the tape. Binders preserve the durability of the tape by keeping the tape from deterioration over a period of time (42; 47).

The two types of binders are polyvinyls and polyacrylates (47). The main difference between the two classes of binders are burn off and removal characteristics. Vinyls need an oxygen atmosphere during the sintering process to completely burn out or oxidize. With acrylics, the polymers disassemble and evaporate. The choice of binder is dependent on the solvent used in the tape recipe (42). Binder concentration must be optimized in any process to achieve high packing order of the particles.

Plasticizers

Plasticizers are the ingredients that make working with tape casting easier, allowing for shaping, cutting, and handling of the green tapes. Plasticizers are additives that enhance binder performance and improve the green tape physical or mechanical properties (48). The function of plasticizers is to allow the green tape to flex and move

without cracking. During manufacturing and handling, the tape must be able to be rolled, formed, and punched. Green tapes that have incorporated plasticizers can endure larger strains than tapes without plasticizers as shown in Figure 8. Green tape can handle a high stress in the elastic deformation range (42; 48). The use of plasticizers makes it possible to roll the tapes for easy storage and allows for blanks to be cut out with no damage to the rest of the tape.

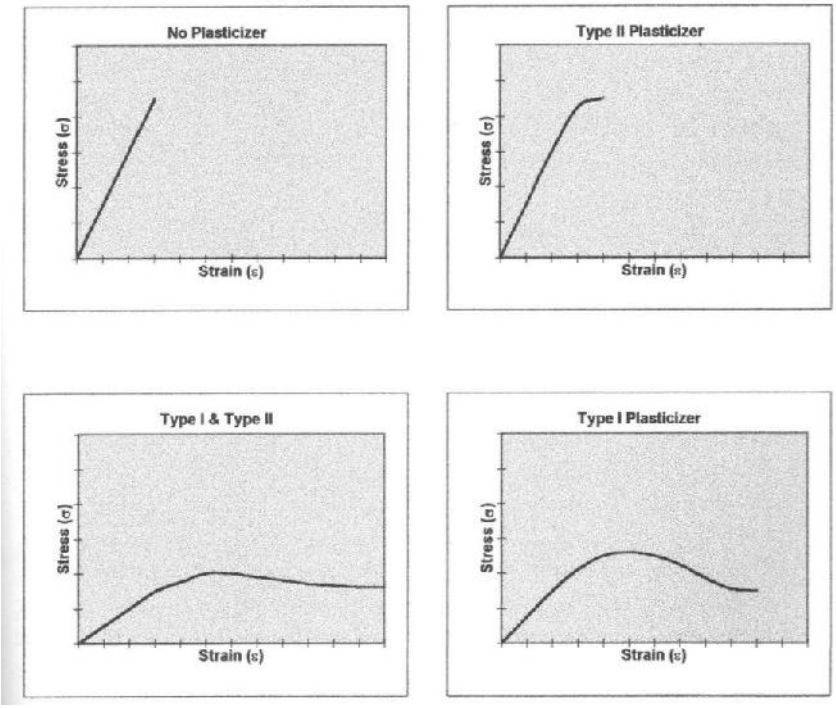

Figure 8. Plasticizer Stress-Strain Properties (10).

The two types of plasticizers used in a tape casting process are: Type I, which promotes flexibility; Type II, which increases mobility of the green tape. The flexibility of Type I plasticizers is a function of their ability to soften the binder polymer chains. Cross linking between the polymer chains is prevented by Type II plasticizers. The main

benefit to Type II is the lowering of the yield stress. It also increases the strain to failure (42).

Sintering

Sintering aids in the creation of SOFC components from the green tapes through a thermodynamically driven process. This process takes place at a lower temperature than the melting point of the material, sometimes as high as 1800°C. During the sintering process, the samples can shrink up to 40% by volume which can be determined and adjusted for experimentally (49). The driving force that allows sintering to occur is the "reduction of surface energy of the particles caused by decreasing their vapor-solid interfaces (43)." The particles in contact with one another will start to fuse together at certain temperatures, forming grain boundaries. Pores between the particles start to close resulting in a denser and therefore stronger part. The porosity of the particles slowly decreases leaving an adequately dense ceramic part with grain boundaries. The first stage of the sintering process is the ramp rate (°C/min) to the maximum temperature. During this period, all of the lubricants and organic materials are burned out of the material (44). The second stage is the dwell time at the maximum temperature to ensure the particles diffuse completely, leaving a fully dense part as shown in Figure 9. The cool down of the specimens for handling, is the last stage in the sintering process (43). The time to reach maximum temperature, dwell at that temperature, and cool down requires expensive ovens and electronic controls. Sintering is a time consuming and expensive process.

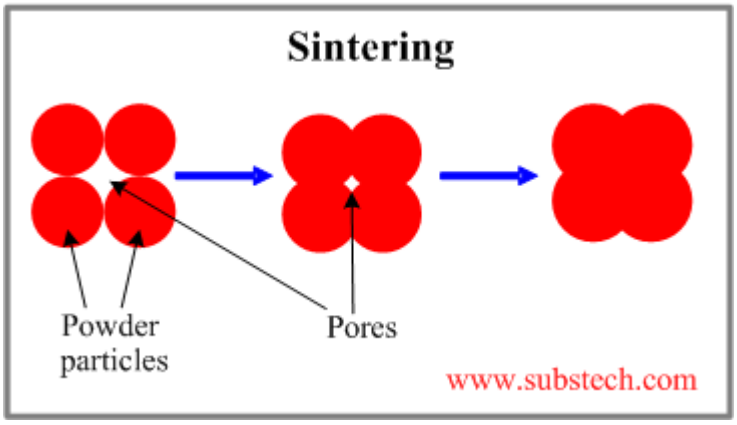

Figure 9. Thermodynamically Driven Diffusion of Particles (43).

If the components of an SOFC could be co-sintered all at the same time the manufacturing cost would dramatically decrease. The electrolyte has the highest sintering temperature to fully densify it and not allow the gases to mix. The electrodes must be porous to promote gas flow to the three phase boundary. LSM will negatively interact with the electrolyte at high firing temperatures around 1300° C (2; 3). By reducing the sintering temperature of the electrolyte the possibility for co-sintering of the MEA becomes possible.

TAPE CASTING CERAMIC PROCESSING

Ceramics must be formed into the desired shape for the intended application. There are many different processing techniques that can be used to achieve various shapes and sizes. Each process requires special ingredients mixed with the ceramic powder to obtain the desired results. The processes discussed will focus on techniques use for SOFC fabrication.

Ball Milling

Ball milling and centrifugal mixing can be used to create electrode inks and electrolyte slurries due to their ability to break up agglomerates through high mechanical sheer. The ball milling process is done in two stages and can take up to four days to complete. In the end, the slurry or ink is a homogenous mixture with desired particle dispersion. Mixing media is placed into a round container with the ceramic power, dispersant, and solvent. The container is then placed between two rollers attached to a variable speed motor for mixing as shown in Figure 10. This is done in the first stage to ensure proper particle dispersion before locking all the particles into position with the binders. During the first stage of ball milling the particles must be fully coated and the polymer bonds must be broken down. Mixing media must not contaminate the slurry and be hard enough to break down and mix the ingredients in the fluid. The size of the media, time of mixing, and speed of the mixture all contribute to achieving a proper slurry.

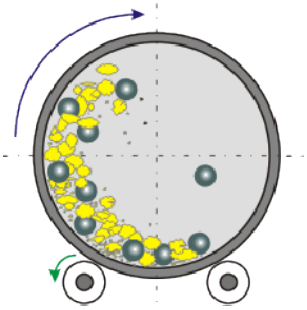

Figure 10. Ball Milling (50)

The second stage of the ball milling process is the addition of binders and the plasticizers to the container to interact with the existing slurry. The mixing process of the second stage must be experimentally established to ensure a homogeneous mixture of all the constituents in the process; this usually takes days. Then duration of the mixing must not be too short or the ceramic will be brittle and weak. The mixing also must not go so long that the binders break down, weakening the polymer bonds. The time constraint for stopping the mixing period has a window for producing optimal slurry. The time window can be established using sedimentation studies. After all the mixing is complete the milling media is separated from the slurry and the ceramic slurry is ready for further processing.

Centrifugal Mixer

The centrifugal mixer makes ceramic slurries in a two stage process similar to ball milling process. Components must be mixed at separate times in order to modify the slurry as designed. The use of a centrifugal mixer eliminates the use of milling media; no separation from the slurry is required and therefore requires little clean up. A container, specially designed to fit within the mixer, contains the slurry. The duration of the

homogenization takes an hour instead of days with this mixture. The container is spun in one direction while a larger rotating platform, holding the container, rotates in the opposite direction as shown below in Figure 11.

Figure 11. Centrifugal Mixing Diagram (Left) (51) Centrifugal Mixer (Right).

There is a degassing step during the mixing process which eliminates the air bubbles and produces a homogeneous mixture free of gas. Once the process is complete, the slurry is in a sealed container ready for a specific process. Small quantities must be used in centrifugal mixing due to the limitations of the counter balance on the main rotating platform.

Degassing

Air can become trapped during mixing of the ceramic tape components. To avoid streaks or voids in a tape during casting, all the larger particles and air must be removed. Once the slurry is made, the contents are poured through a fine mesh filter into a separate container and immediately placed into a vacuum chamber. The chamber is then pumped down until gas bubbles appear and then vented. This procedure is followed until bubbles

cease to appear in the electrolyte slurry. The pressure cannot become too low in the chamber or violent eruptions of air will cause loss of material and a mess in the vacuum chamber.

Uniaxial Pressing

Uniaxial pressing is used to press ceramic powders into simple shapes such as a disk or cube using a single direction on motion. Minimal amounts of plasticizers and binders can be added to the powder before pressing to enable handling of the pressed part prior to sintering. Mechanical or hydraulic means are used to press samples. Pressing can be done at room temperature or elevated temperature to increase density and improve particle packing (52). A lubricant is used on the inside of the die to reduce the friction when removing the finished part and to minimize density gradients through the pressed ceramic samples (32). The three stages of pressing, as shown in Figure 12, are: (1) fill die with determined amount of powder and additives, if necessary; (2) compress the green material; (3) remove the press formed part.

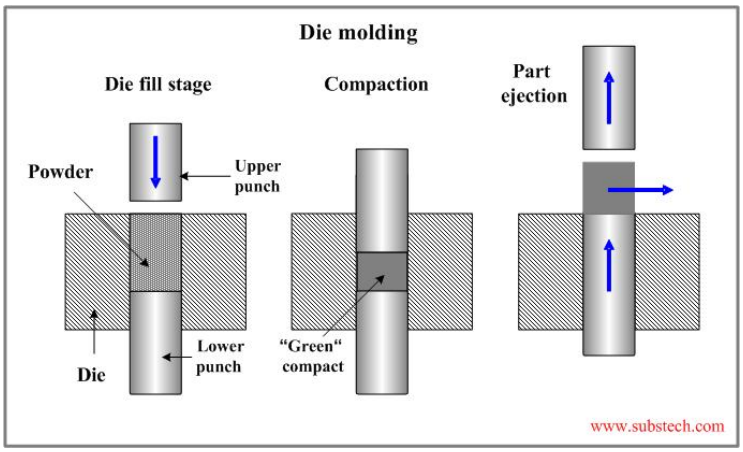

Figure 12. Uniaxial Pressing (52)

While under compression, the particles first fill all the vacancies present then the bonding of the particles starts to occur. The pressures often used to create parts are between 2,000 and 120,000 pounds per square inch (psi) (52). When the process is complete the part should remove from the die easily with the ability to be handled without cracking or breaking before sintering.

Tape Casting

Tape casting of slurries is a process to produce thin, continuous ceramic tapes. The tape thickness is dependent on the doctor blade height and the amount of slurry in the reservoir which produces hydrostatic pressure. A carrier material, usually a non-stick polymer for easy tape removal, is used to pull the slurry under the doctor blade and onto the flat surface. The length of the tape can be processed to be shorter than the casting bed. This is called batch casting. Batch casting was used exclusively in the electrolyte manufacturing process. The substrate can be left on the surface until the solvents dissolve and dry, leaving a workable ceramic tape. A continuous method, used in industry allows for the ceramic to be pulled over a long tape casting table slowly in order to dry before being collected on a take-up reel, shown below in Figure 13.

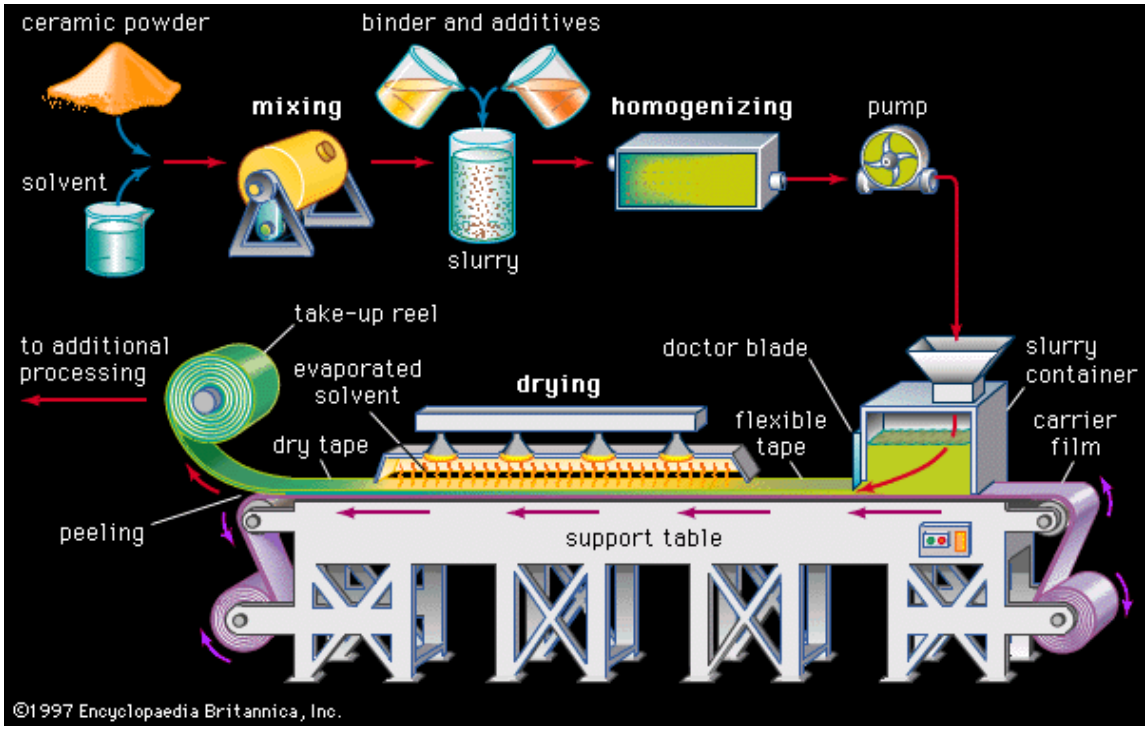

Figure 13. Tape Casting (53)

Slurry preparation, as discussed earlier, produces a homogeneous ceramic mixture that has been filtered of all undesirables and purged of most of the trapped gases prior to tape casting. Laboratory casting is completed by filling the doctor blade reservoir by hand with small sample sizes. The laboratory tape casting table use to create the this ceramic membrane is shown in Figure 14. The fluid level can physically be monitored so sensors are not needed. Many variables determine the final characteristics of a tape. The slurry must be prepared specifically for the desired outcome. Doctor blade height, carrier speed, and reservoir height must all be determined prior to tape casting. Along with a precise casting process, the slurry must have a homogenous mixture with an optimum viscosity to produce a simple, thin ceramic electrolyte. The temperature of the table can also impact the casting process. Temperature can be beneficial because cold beds can control porosity and warm beds for improve drying time.

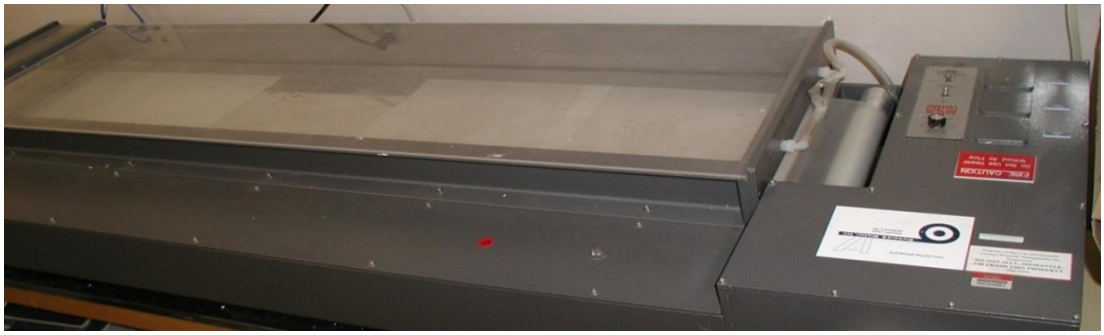

Figure 14. MSU Tape Casting Table

Equipment

For the laboratory processing, a Mylar polymer carrier sheet was used to advance the hand-poured slurry along the precision machined granite slab for a smooth tape. Two different types of doctor blades could be used for this process. A single or double doctor blade with different widths could be used for processing. The doctor blades have micrometers to adjust the thickness of tape. The doctor blades must be light weight to allow a carrier sheet to be pulled under them. These are shown in Figure 15.

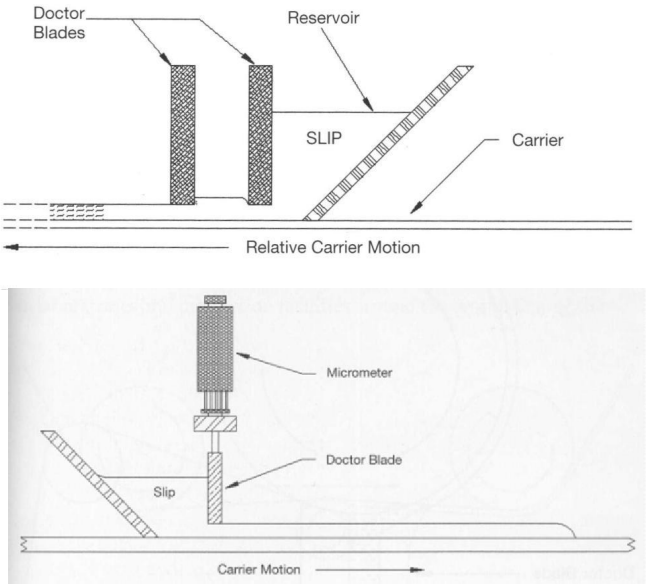

Figure 15. Double Doctor Blade (Top) Single Doctor Blade (Bottom) (42)

When using a single blade, the fluid height must be kept constant to keep the tape at a consistent thickness for the entire length. This process works best when the batch sizes are small. To eliminate small error in tape size from hydrodynamic forces, a dual doctor blade can be used. The first blade feeds a constant level of fluid to the second blade producing even tape thickness. Tape thickness for ceramics are on the order of 120 to 1000μm (0.0047 to 0.040in). Doctor blades are used in all ceramic tape casting. They must not interact with any of the ingredients of the slurry (42). Easy removal of the blade aids in the clean-up process, which must be through after every batch.

The viscosity of the fluid must be such that it can flow with the speed of the carrier sheet to keep the fluid at the exact height of the blade. If the speed is too slow, the hydrostatic pressure from the reservoir will cause the slurry to come out thicker than the blade is set (welling). If the speed is set too fast, the fluid will be thin and spread unevenly. The rate of movement should not be altered during a cast for consistency of tape characteristics.

Drying

After the tape is cast the solvents must evaporate and a sufficient amount of time must past for the tape to dry. Aqueous solutions take longer to dry than organic (non-aqueous) solutions. Diffusion of the solvent through the thickness of the tape is the limiting factor on the drying time. All of the solvent must migrate to the top of the tape to evaporate. This one-sided drying is due to the sheet preventing evaporation at the bottom of the tape (42). To speed up the process, the MSU tape casting table uses the aid of air convection to evaporate the solvents. Generally, a tape will shrink after the drying

process and this shrinkage must be accounted for when adjusting the doctor blade height. Common tape deformations from the drying process can be seen in Figure 16.

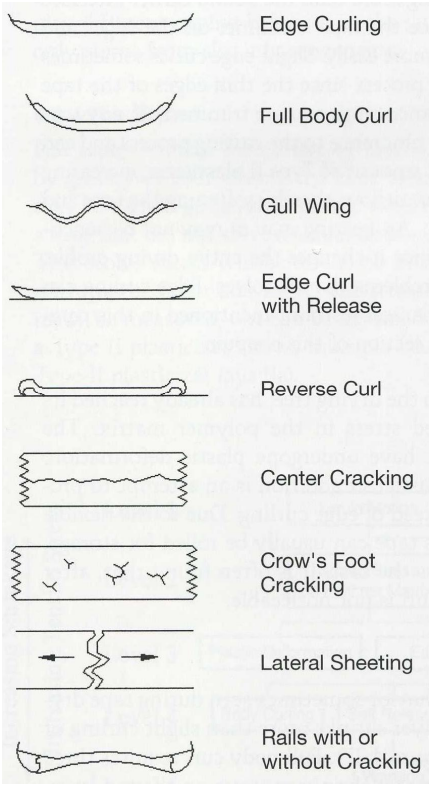

Figure 16. Dry Tape Imperfections (42)

Removal from the carrier sheet is not necessary immediately after the drying process. It can be completed prior to the sintering process. After the dying process is complete the tape is able to be rolled for storage or cut into working pieces.

REDUCING SINTERING TEMPERATURE

Sintering of the ceramics can take place at temperatures as high as 1800°C to produce completely dense ceramic parts. The electrolyte in a SOFC needs to be a dense hermetic membrane for the cell to function properly which typically requires densities exceeding 93% of theoretical (33). Reducing the sintering temperature of the ceramics will help reduce the time and cost of producing commercial SOFCs. Alternate methods have been investigated in the reduction of sintering temperature. Many include the use of nano-particles and transition metals.

Nano-Particle

Sintering is a thermodynamically driven process characterized by the free surface energy of the particles involved. With nano-scaled powders, the particles have much greater surface areas than micro powders. The energy at the surface of the particle is higher than the grain boundaries that are in contact between other particles. To achieve a lower surface free energy state, nano-particles will start lattice diffusion. This diffusion will cause the material to densify. Nano-particles can achieve a higher packing order than micro powders, resulting in a higher green density. The lower porosity of the higher density samples have increased activity during sintering (54). This creates a faster onset of temperature for sintering and can be achieved at lower temperatures. Nano-particles increased surface area can lower the sintering temperature for YSZ. However, the complication when working with small particles is overcoming the agglomeration of the

particles for processing; small clusters of the powder tend to bond and resist mechanical agitation for separation.

Transition Metals

The addition of transition metals, in trace amounts, to YSZ can lower the sintering temperature of ceramics. Published research suggest that the addition of copper oxide as a transition metal in amounts less than 1 mole % increased the sintered density of 8YSZ in a temperature range of 1250°C to 1500°C. The lowest temperature, 1250°C, showed the greatest increase in the sintered density of the doped samples over plain YSZ (55). Since nickel is readily available for production of anode material in SOFC fabrication, nickel oxide is a viable, inexpensive option for transition metal sintering enhancement.

ANALYSIS TECHNIQUES

To support in the validation and understanding of the effects that nickel oxide dopant contributes to YSZ many analytical techniques were used. The use of a scanning electron microscope (SEM) enabled detailed imaging for close inspection of ceramic microstructure. Additionally, various effects of temperature on ceramic processing were examined using a dilatometer. An INSTRON machine, used in conjunction with a concentric ring mount, accurately tested the mechanical strength of the brittle electrolyte.

Scanning Electron Microscope

Scanning electron microscopes use electrons to form images instead of light. A highly focused beam of electrons is scanned across an area of the sample exciting the secondary, low energy electrons on the surface of the material. This must be contained under vacuum. Image mapping on an SEM is formed from detection of electron intensity as a function of position as the electron beam scans the sample, as shown in Figure 17. Low electron energies and low penetration depth makes a high magnification of x100,000 possible while retaining high resolution. (56; 57)

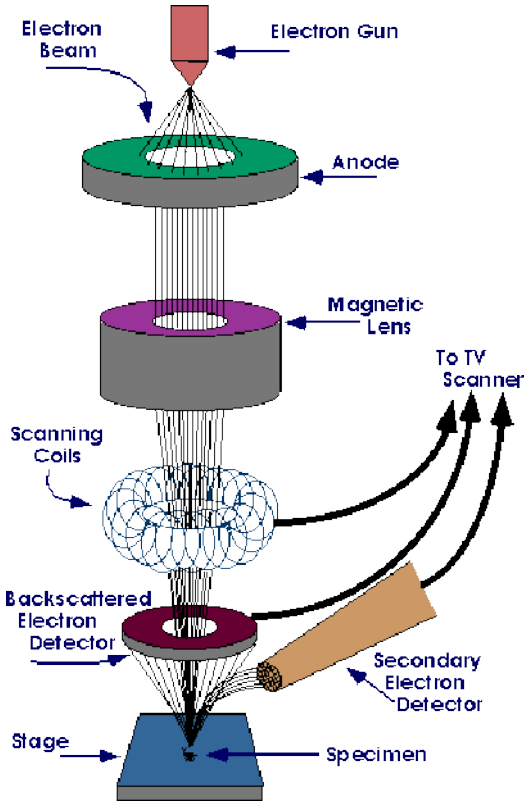

Figure 17. SEM Diagram (56).

Dilatometer Analysis

Samples are placed on a support centered in a furnace. A predetermined, minute pressure is applied to a probe. This probe measures the change in length of the sample during a thermal cycle with a sensitive position transducer, as shown in Figure 18 (58). The expansion or contraction of the specific material is used to determine its coefficient of thermal expansion. Dilatometer analysis can determine the rate and onset temperature of sintering for the material of interest.

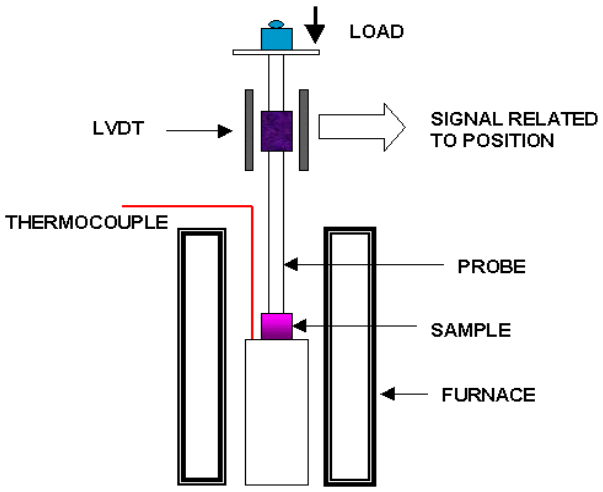

Figure 18. Dilatometer Diagram (58).

Impedance Spectroscopy

Electrochemical impedance spectroscopy (EIS) is a method for determining electrical characteristics for a material with solid-solid or solid-liquid interfaces (59). Electrochemical impedance spectroscopy is an ideal method for characterizing SOFC components. Steady-state electrochemical parameters of interest include bulk and grain boundary diffusion coefficients. The common method used for EIS is done by applying a known current or single-frequency voltage and measuring the phase shift and amplitude as the frequency is varied. EIS test rigs coupled with oscilloscopes can measure the impedance or AC resistance as a function of frequency ranging from 1mHz to 1MHz (60; 59). The impedance is dependent on the frequency, such that the response of the system indicates how the mechanisms are occurring (59). With the use of computer software the functions are plotted and easily analyzed for electrochemical properties.

When dealing with the YSZ electrolyte EIS helped determine the contribution the nickel oxide dopant had to on grain interior and grain boundaries.

INSTRON Testing Machine

The INSTRON materials testing rig is capable of performing tension, compression, fatigue, and hardness strength tests. Sample displacement and the force necessary to cause displacement is monitored and recorded to calculate ultimate yield strength. Brittle ceramics' yield strength are highly dependent on loading methods due ceramic characteristics of experiencing fracture before the yield strength is ever reached (32). Therefore, a concentric ring fixture was used to evenly distribute the applied force, providing consistent failure distribution. The load ring applied an evenly distributed continuous force over a large portion of the sample until failure. With the ASTM standard C 1499-05 the test is indicative of the bulk material property. The ring-on-ring loading negates the edge fracture of the sample (61). The details of the concentric ring will be discussed later.

EXPERIMENTAL PROCEDURE

Experimental Problem Definition

The research was conducted to attempt to decrease sintering temperature of traditional YSZ in the electrolyte of an electrolyte supported fuel cell using low levels of nickel oxide dopant (NiO). Manufacturing cost and chemical interaction will decrease with a decreased sintering temperature. The design objectives are: (1) optimize slurry batches and tape casting process to produce constant, repeatable electrolytes for fuel cells; (2) identify the mechanical behavior as a function of sintering temperature and dopant concentration; (3) identify potential mechanisms of sintered enhancement of doped YSZ utilizing mechanical and electrical property data.

Nickel Considerations Study

Preliminary sintering studies were done with 8 mole % YSZ (Tosoh Corp, Lot # S805603P) with four different types of nickel dopants mechanically mixed in. The dopants were added in 0.5 mole % increments up to 1 mole % to the YSZ micro powder. The four dopants used were: (1) black nickel oxide powder (Ni 76%, Alfa Aesar, Lot # E11Q23) (2) green nickel oxide (99%, Alfa Aesar, Lot # C01R011) (3) nano grade black nickel oxide (Inframat Advanced Materials, Lot # IAM9014NNIO) (4) nickel nitrate (Alfa Aesar, Lot # 10109280). The powder was then dry pressed into half inch diameter pellets and sintered for one hour at 1400°C. The geometric density was calculated as grams per cubic centimeter to determine the highest density compared to the theoretical

density. Relative density is a ratio of published values with perfect crystal structures compared to experimentally determine values and is shown below in Equation 1.

$$\%\ Theoretical\ Density = \frac{Experimental\ Value}{Published\ Value} X100$$

Equation 1. % Theoretical Density

The precursor nickel dopant displayed the best sintering advantage and was chosen as the test dopant due to the performance, availability, and price. The amount of dopant added to the YSZ powder was also determined. Nickel oxide was added to both 3mol% YSZ (Tosoh Corp, Lot#8306607P) and 8mol%YSZ in amounts of 0.1, 0.5, and 1.0mol%. The correct amounts of powder were measured for a 25 vol% of solids suspension. A surfactant was used to disperse the two powders. The dispersant was an ammonium polyacrylate surfactant (Darvan C-N, R.T. Vanderbilt Co., Inc., Norwalk, CT) in the amount of 1 weight %. Homogenization of the slurry was achieved via a centrifugal mixer (ARE-250, Thinky Corporation, Laguna Hills, CA) run for five minutes at 1000 revolutions per minute.

To preserve the slurry homogeneity during the drying process the powders were frozen via liquid nitrogen. The frozen mixture was then placed into a countertop freeze dryer (Virtis Advantage, Virtis Co., Gardiner, NY). Utilizing a 10mT vacuum at 40°C, the water was sublimated from the slurry leaving a free flowing fine powder. The powders were then pressed with a uni-axial press. Powders were poured into a 1.27 cm stainless steel cylindrical die and pressed with a pressure of 27.5MPa. The pressure was maintained on the die for one minute at which time it was released slowly to prevent spring back or breakage of the part.

8mol% and 3mol% YSZ with doped and undoped powders were all pressed and sintered in a tube furnace under ambient conditions at 1200, 1300, and 1400°C for one hour. The undoped samples were for a base line density comparison to the doped samples. All the pellets were weighed and measurements of the diameter and thickness were taken prior to and after the sintering process. The green and fired geometric densities, determined using Equation 2, were all calculated for comparison.

$$\rho(density) = \frac{mass}{\pi * thickness * radius^2}$$

Equation 2. Geometric Density Calculation (g/cc)

Particle Size

Manufacturing data was not available on two of the nickels used in the sintering study. The Alfa Aesar black nickel oxide and Alfa Aesar green nickel oxide particle size was determined using a laser scattering particle analyzer (Zetasizer Nano-S90, Malvern Instruments, Worcestershire, UK). A solution consisting of 20 milliliters (mL) with 0.1 millimoles per liter (mM) sodium chloride (NaCl) with 0.1 moles per liter (M) creating a medium in which the laser can penetrate while maintaining actual particle size. The analyzer was then operated in accordance with the operating manual. Nano particles were negated for further investigation due to the difficulty of working with them. Small particles tend to clump together making clusters that are difficult to disperse in a solution. For a reliably repeatable process, were used macro particle powders for dopants and YSZ.

Dilatometer

A dilatometer with a vertical alumina tube (L75, Linseis, Robbinsville, NJ) was used to sinter small sample pellets of the two different powders to determine onset temperature of sintering. A baseline test was performed under ideal conditions to compare the nickel oxide doped samples of micro-powder YSZ. The dilatometer runs were done with ambient air flow from room temperature to 1400°C at a ramp rate of 10°C/minute. Samples dwelled at the max temperature for one hour and then were cooled down to 1000°C at 30°C/minute; cooling continued to ambient temperature at a rate of 20°C/minute.

Impedance Spectroscopy

To ensure that the amount of nickel oxide that was added to the powders did not alter the electrical performance, an impedance spectroscopy unit (5897 Impedance Analyzer, Solartron Analytical, Farnborough, Hampshire, UK) was utilized. A comparison of ionic conductivity was conducted using doped and undoped samples specifically chosen and prepared with silver contact leads and paste. Each face of the 1.27cm pressed samples were pasted with silver. Leads were placed on the sample during the drying time of the paste to secure the leads to the specimen. Samples used for the test had been sintered at 1400°C or 1300°C for one hour prior to the silver paste application.

Each test sample was then heated in the conductivity test rig to 850°C under ambient air flow with a frequency sweeping from 1Hz to 10 MHz. During the frequency

sweeps the sample was cooled in increments of 50°C until room temperature was reached. Once the first stage of the conductivity testing was completed a second more refined test was run. Each sample was heated to 500°C and cooled to 240°C during the same frequency sweep. Nickel is electrically conductive and will transfer electricity if a high concentration of nickel oxide is present in the electrolyte. The electrolyte must be completely free of electrical conductivity. The higher the ionic conductivity of the ceramic the more efficient the SOFC will become. Trace amounts of the nickel oxide dopant were used to limit the possible negative ionic resistances while enhancing the sintering of the YSZ.

Sediment Study

A dispersion test was run to determine proper weight percent of a fish oil to optimize dispersion in a nickel oxide solution and an 8YSZ solution. Testing was also performed on 8YSZ slurries to investigate the most efficient mixing speed in a THINKY ARE-250 centrifugal mixer. Samples were left undisturbed on a level surface for five days before being analyzed.

Centrifugal Speed

Base line tests were run to find the optimal rpm speed for mixing 8YSZ powder in solvent and dispersion solutions. 10 grams of YSZ were added to 6.67 grams of 60/40 Xylene/Ethanol solution and 0.23 grams of blown menhaden fish oil dispersant (Richard E Mistler, Inc Lot # 29215). The ingredients were mixed in a container designed for a THINKY ARE-250 centrifugal mixer and mixed for five minutes at 2000, 1500, 1000,

and 500 rpm. After mixing the slurry was poured into a test tube then capped and placed upright to settle.

Dispersion Study

Blown menhaden fish oil (MFO) dispersant was used with both 8YSZ and nickel oxide samples. The dispersant was added from zero to six weight percent of the powder. Each small sample was mixed using a centrifugal mixer running at 1500 rpm for 5 minutes then poured into a test tube to settle. After seven days the samples were compared visually to determine optimal levels of fish oil.

Samples were made with 15 grams of either 8YSZ or nickel oxide powder. Next, a mixture of 10 grams consisting of 60/40 Xylene/Ethanol solvent was added to the powder. The slurry was then mixed as described above and set aside to let particles settle out. It was determined that the optimum weight percent for fish oil is 2.26 for this research.

Centrifugal Mixing

The mole percent of slurry constituents, found through the use of the sediment study, must be mixed together. Combining the ingredients and producing a homogeneous mixture was accomplished utilizing a centrifugal mixer. The slurry was manufactured in a two stage process consisting of either 8YSZ or 3YSZ. Each powder was used with and without the nickel oxide dopant to give four distinct slurry recipes. In the first stage of an undoped slurry sample, the desired powder was chosen. Forty grams were measured out into a container specifically designed for the THINKY ARE-250 centrifugal mixer. The mixer has a counter balance to keep the rotation of the internal platform smooth, limiting

the sample weight that can be mixed. Adjusting the counter balance is dependent on the combined weight of the sample to be mixed and container. All the ingredients contained in the slurry are based off the weight percent of powder used. A solvent of xylene and ethanol in a ratio of 60/40 weight percent was added to the container by 40 weight percent of the powder. This required 26.67 grams of solvent. The fish oil dispersant with 2.26 weight percent resulted in the addition of 0.904 grams to the total weight of the slurry. If a nickel dopant was to be added to the solution it was included in the first mixing cycle. Adding 0.337 grams of the nickel oxide was equivalent of one mole percent of the YSZ powder weight.

The slurry enclosed within a container was then weighed on a digital scale and placed into the centrifugal mixer. The counter balance was then adjusted accordingly before the lid was closed on the mixer. A program was set to run at a desired speed for an allotted time. After many trials, in conjunction with the sediment study, the program for the first mixing cycle was optimized to four minutes at 1000 rpm for 8YSZ and four minutes at 1200 rpm for 3YSZ. The consistency of the slurry after the first stage resembled that of water but white in color.

For the second stage of mixing 3.20 grams of Polyvinyl Butyral B-98 binder (Richard E. Mistler, Inc Lot #T43343), 2.0 grams of Butyl Benzyl Phthalate S-160 Type I plasticizer (Richard E. Mistler, Inc Lot # DC086807), and 1.60 grams of Polyalkylene Glycol Type II plasticizer (Richard E. Mistler, Inc Lot # SC1955S3DI) were added in 8, 5, and 4 weight percents, respectively. The binders and plasticizers were hand mixed in a separate container to achieve a small level of homogeneity before being hand mixed into

rest of the slurry. This was to speed up the mixing process of the second stage, as well as produce repeatable samples. A second stage of centrifugal mixing followed the hand mixing. The entire container and contents were weighed and placed into the THINKY, the counter balance was set, and the program was run. 8YSZ required 15 minutes at 1000 rpm followed by a 5 minute, 600 rpm degassing run. 3YSZ needed a higher mixing speed, which was programmed as 15 minutes at 1100 rpm and degassed for 5 minutes at 600 rpm. Second stage slurry batches produced a homogeneous mixture with desirable viscosity comparable to that of cooking oil. The final mixing programs were also based off of the sediment study and experimental trial and error. Many iterations of the mixing process were required to produce a well homogenized slurry with desirable flow properties. Trial and error iterations helped in part to determine powder weight, mixing parameters, and hand mixing steps.

Hand Mixing

Hand mixing of the slurry ingredients is vital to producing repeatability, homogeneity liquid ceramics. The binders and plasticizers are first mixed by hand with a wooden dowel in a separate container before being added to the slurry. This step creates a compound of plasticizers and binders instead of three distinct ingredients. The compound is then added to the previously prepared slurry and hand mixed again via wooden dowel. Hand mixing the second time disperses the compound in the first stage slurry to prevent large clumps from forming during the centrifugal mixing stage.

Hand mixing was required for shorter durations during the mixing programs and produced repeatable results. Without hand mixing, some of the binder clusters would never dissolve, leaving an unusable slurry regardless of the centrifugal mixing regime. Hand mixing used in conjunction with the centrifugal mixer produced desired slurries.

Tape Casting

Tape casting involves many steps such as proper preparation of the slurry samples and doctor blade manipulation. Factors such as curing time had to be examined to produce repeatable, uniform ceramic tapes.

Sample Preparation

The slurry made using the mixer was placed into a drying oven (Lindberg/Blue M Model # 601305A-1) set at 70°C for a 24 hour period. Heating the slurry melts and disperses the binder's particles that are too fine to be detected via visual inspection. The heating process is vital and was deemed necessary during the tape casting process. Tiny pin holes were forming throughout the entire tape after the drying process of the tape was complete. Pin holes are a problem because the electrolyte must be completely dense for an SOFC to work. Alterations, such as binder, plasticizer, and dispersant levels were made to the slurry batch makeup to negate the problem. These did not remedy the problem. Different mixing speeds and duration in conjunction with different casting techniques failed to provide a dense ceramic tape. The polymer binder was found to disperse more thoroughly with the addition of heat. Once the slurry was held at an

elevated temperature (70°C) for a long enough period of time, the cast ceramic was solid after the drying phase.

Doctor Blade

A 10.16cm wide single aluminum doctor blade was used to cast the ceramic tapes. An aluminum design was used to ensure no reaction of the ceramic slurry with the doctor blade would occur. The blade height was determined experimentally due to the tape shrinkage during the drying period to produce tapes with thicknesses close to those of commercially available tapes that are 120µm (micrometers). Doctor blade height was optimized at a height of 450µm leaving a tape thickness of 120µm after the curing process was complete. Iterations of blade height from 400-500µm were investigated to match manufactured tape thickness resulting in 450µm as the desired thickness. The doctor blade micrometers have settings of mils ("milli-inch"), so a conversion from mils to micrometers, or microns, was needed, as shown in Equation 3.

$$1\ micron = 25.4\ mils$$

Equation 3. Micrometer to Mil Conversion

The adjustment of the blade height was completed on the surface of the precision machined granite table top of the tape casting machine (Richard E. Mistler, Inc.). Fine adjustments in mils were set to achieve the desired height. After all the adjustments were made, the doctor blade was placed on top of the Mylar carrier sheet. The speed of the Mylar sheet was set to 40 percent of the tape casting machine's maximum speed. Carrier speed determined the rate in which the slurry was poured into the reservoir of the doctor blade to maintain a constant level and controlled fluid flow.

Curing Time

The ceramic tape was short enough to stay on the tape casting table during the drying period. The ceramic slurry was left for 24 hours to dry. Air convection was used to aid in the drying of the non-organic solvent mixture. Once the tape was cast and stationary, a vacuum was turned on to pull air over the thin sheet. Air movement was applied after the process was complete. This helped to remedy the inherent problem of the tapes drying too quickly during the pouring process, causing surface deformations. Upon completion of drying, the Mylar sheet was cut at the ends of the casted tape and the tape was rolled and labeled for storage.

Sintering

A 5.397cm die was used to punch six samples from tapes with and without nickel oxide dopant. The twelve samples were then sandwiched separately between two 25.4cm x 27.94cm x 0.9525 cm aluminum oxide plates. Samples were spaced, so no contact would occur, with a total pressure of approximately 113 Pa applied. The pressure was used to ensure the samples would stay flat during the sintering process. If no pressure was applied, the samples would tend to develop a wave type surface. The surface of the samples had to remain flat to achieve accurate results during material strength testing. The surfaces of the alumina plates were lightly sanded with 1000 grit sand paper after each run to remove any residuals left from the previous sinter cycle. Samples of both the 8YSZ and 3YSZ, along with their doped counterparts, were tested in this manner.

A box oven (Applied Test Systems, Inc. Kanthal Super 33) was used to achieve the three different temperatures that the ceramic samples would need to reach to fully sinter. Each heating cycle was set up to ramp at 2.5°C/min until the desired temperature was reached. The maximum temperature would remain constant for two hours at either 1300°C or 1400°C. When the maximum temperature was set to be 1250°C the dwell time was increased to five hours.

Density Study

A geometric density study was used to examine the green and fired tape characteristics of doped and undoped tape samples. Density was determined using Equation 1, utilizing the geometry and weight of the samples. The geometric approach was chosen over Archimedes Principles' because the geometry was simple and the density could be determined with relatively high accuracy in a shorter amount of time.

The green density, samples were sandwiched between two glass slides of known thickness and measured using micrometers. The glass slides negated the issue of tape deformation from the micrometers during the measuring process. After the readings were taken, the thickness of the slides was subtracted from the total thickness to give an accurate sample thickness. All of the samples were of circular geometry and the diameters were measured in two different locations and averaged for each sample. Weighing of the green tape in grams was done on a digital scale to an accuracy of three decimal places. Total volume of the samples were calculated and used in Equation 1 to determine the green density.

After the firing process of the tapes, the sintered density was found in the same way as with the green tape. However, glass slides were not necessary for these because the samples were rigid enough to not deform during the measuring of the thickness. Density was determined for all of the doped and undoped tapes of 8YSZ and 3YSZ.

Ring on Ring

The thin ceramic disks were tested only in compression because of the inherently weak characteristics of ceramics in tension. A concentric ring-on-ring test rig, as shown below in Figure 19, was used to test for the mechanical strength. The rings were manufactured in compliance with the ASTM standard C 1499-05 to apply a distributed monotonic uniaxial load on ceramic membranes at ambient temperature (61). To fit into the ASTM guidelines the ceramic samples had to be isotropic on a macroscopic scale and monolithic. Ring-on-ring testing helps to limit the edge effects of the samples where the stress is the weakest. This type of testing proved to be very useful for comparing materials such as doped and undoped YSZ samples. Ceramic strength is greatly dependent on flaws and other surface defects. To negate this problem, multiple samples were tested and averaged. Each of the four different tape recipes had 18 samples tested at each of the sintering temperatures.

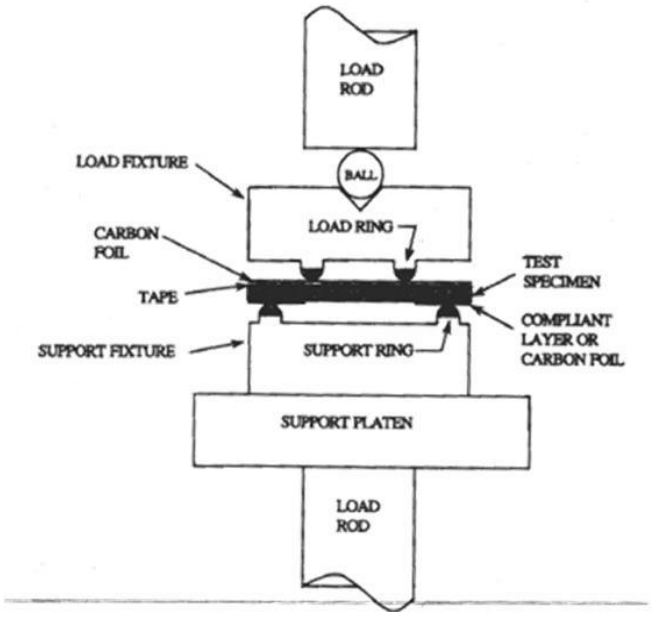

Figure 19. Ring on Ring Schematic for Equibiaxial Testing (61)

The top load rod of the fixture was placed and pinned into the top of a 5500 series bench top INSTRON load frame. The bottom of the INSTRON load frame held and secured the bottom load rod with the aid of a pin. A support ring was then placed on the support platen. The support ring had a hole in the bottom that fit over a raised cylinder, which was machined into the support platen to restrain the support ring movement during testing. A sample, visually inspected to be free of surface contours and defects, was placed onto the bottom support ring. The top load ring was then carefully stacked on top of the electrolyte sample. The load ring had a centered channel machined into the top to hold a 0.792cm steel ball bearing. Ball bearings are used to evenly distribute the weight of the top load rod during the uniaxial test. A notch was also machined into the top load rod that was 0.601cm deep and 0.601cm in diameter to fit the steel ball bearing. The ring on ring components were all made from 6061 T-6 aluminum.

Procedure

Prior to testing the electrolyte samples the diameter and thickness were measured and recorded for analysis. Thicknesses and diameters of the samples were measured with digital calibers with a resolution of 0.01mm at two different locations and averaged. Each sample was visually inspected to ensure the surface was free from contours and cracks. Samples were then placed on the clean support ring with a slight overhang. The clean load ring was then carefully centered over the ceramic part.

The entire apparatus was preloaded to 10% of the failure load of the electrolyte. INSTRON data acquisition software (BlueHill) was used to control the compression of the samples at a selected displacement rate of 2mm/min until reaching failure. The displacement of the ceramic was recorded as a function of force. Once failure occurred, the sample was pieced back together, if possible, and inspected for mode of failure according to ASTM method C 1499-05, as displayed in Figure 20.

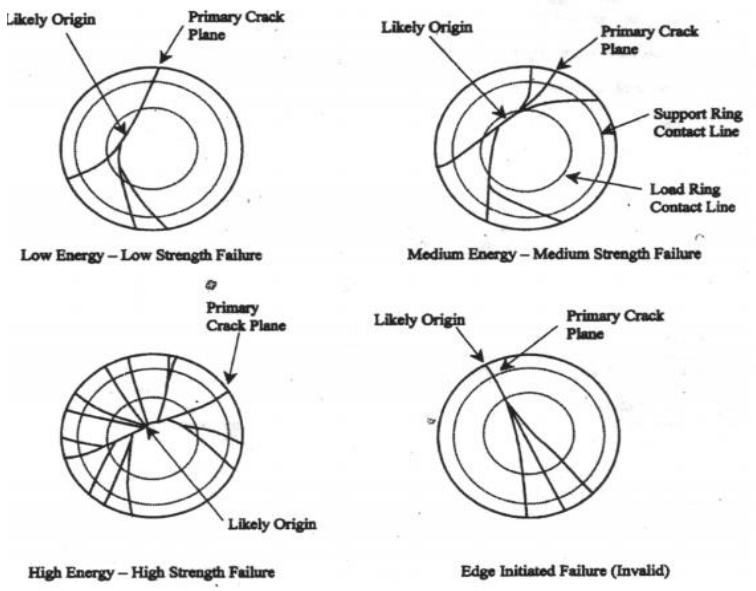

Figure 20. Mode of Failure Characterization in Concentric Ring Test Specimens (61).

Strength Results

Data from the strength of failure and displacement was used to compare the different electrolyte tapes on a failure strength basis. Equibiaxial strength is σ_f (MPa), F is the breaking strength (N), and D (mm) is the sample diameter measured with digital calibers. The diameters of the support ring and load ring are D_S (mm) and D_L (mm), respectively. The sample thickness (mm) is h, and Poisson's ratio, a dimensionless quantity, is dependent on the material tested. In the YSZ study, a Poisson's ratio of 0.31 was used (62). Diameters for the testing rig were 35mm and 14mm for the support ring and the load ring, respectively. The fracture strength was recorded from the INSTRON machine for each tested sample. The equation to determine the equibiaxial failure strength for a concentric ring on ring test of a circular sample is shown in Equation 4.

$$\sigma_f = \frac{3F}{2\pi h^2}\left[(1-\nu)\frac{D_S^2 - D_L^2}{2D^2} + (1+\nu)ln\frac{D_S}{D_L}\right]$$

Equation 4. Equibiaxial Strength of Concentric Ring on Ring Testing of Circular Samples (61).

Scanning Electronic Microscope

Sputter Coating

Once the electrolyte disks were fractured in the INSTRON machine the small pieces were inspected in a scanning electron microscope (SEM). The fractured edge of the ceramics were fixed to a mounting bracket with carbon tape and placed into a sputter coater. Gold was used to coat the ceramic parts to prevent charging of the material. Sputtering was done for three minutes at 30mA of current in a vacuum chamber.

Image Capture

Images were taken of doped and undoped samples from both 8YSZ and 3YSZ tape recipes. The SEM was set to an acceleration voltage of 20mV, at which point the filament current was saturated to approximately 1.8A. Two magnifications were used on every sample while a low setting of 2000 times magnification was used to get a general overview of surface contours and density. A high setting of 12000 times magnification highlighted the grain size and grain boundaries of the samples.

Modes of failure and grain size are derived from the micrographs taken from the fractured edge of the tape. Transgranular and grain boundary failure were possible modes of failure influenced by nickel dopant. A comparison of grain growth for the tapes sintered at 1250°C, 1300°C, and 1400°C with and without nickel dopant was done at the micro scale of 2000x and 12000x magnification on the SEM. Grain size is determined using the intersecting line method indicated by the two 10μm to scale red lines located on all 12000x micrographs. The grain boundaries were added along each line and divided by the known length of the line. The averages were taken to estimate the different grain size of YSZ and Ni-YSZ at different sintering cycles.

RESULTS

Nickel Consideration

The initial sintering study with pressed pellets showed that the black nickel oxide (Alfa Aesar Lot # E11Q23) was the optimum dopant for achieving higher densities during sintering, as shown in Figure 21. Particle size analysis of the black nickel oxide determined the particle size to be 400nm. Manufacturer (Tosoh) data listed the 8YSZ and 3YSZ average particle sizes to be 360nm and 350nm, respectively.

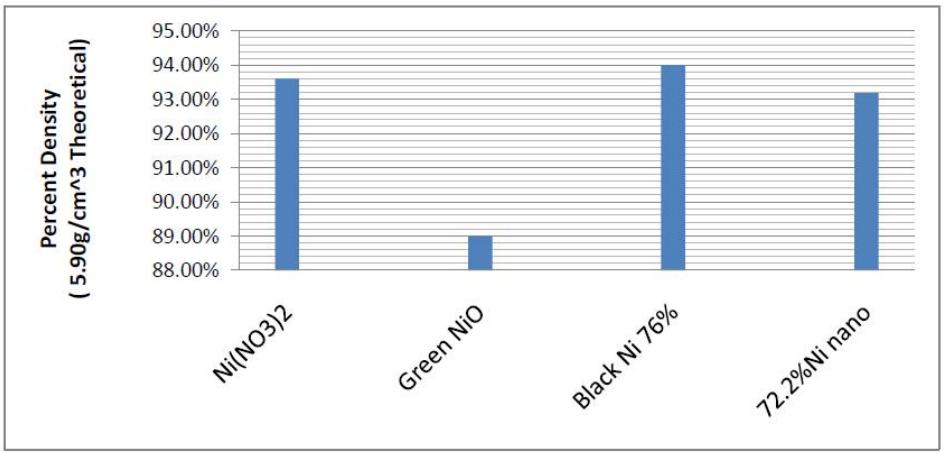

Figure 21. 8YSZ Doped With 0.5mol% Nickel Density Comparison

The small deviations in the particle size between the dopant and the host powder aided in the sintering characteristic of the YSZ. Particle size deviation promotes tight packing of smaller particles into spaces created by larger particles. The other nickel powders had nano particles which did not reach as high of density as the macro powders as shown in Figure 23. Higher packing order of the particles is achieved when the particle size has minimal variation. Density is proportional to the packing factor. For the rest of the studies, black nickel oxide was used extensively.

Sintering Study

Relative theoretical densities were found for both 8YSZ and 3YSZ samples sintered at 1300°C for one hour. Nickel oxide was added in quantities of 0, 0.1, 0.5, and 1mole percents to 8YSZ and 3YSZ. Sintered 8YSZ samples were compared to the reported density value of 5.9 g/cm^3. 3YSZ has a theoretical density of 6.10g/cm^3 and the sintered samples were compared to the published value shown in Figure 22. (63)

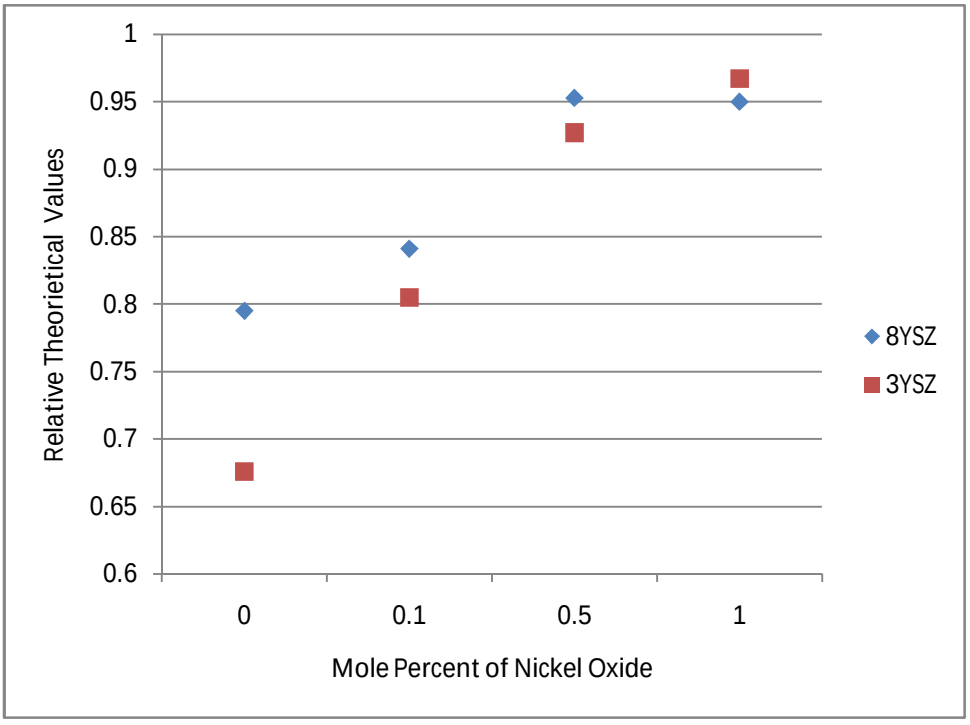

Figure 22. Relative Theoretical Density of YSZ Powders Sintered at 1300°C for One Hour

In a comparison of 8YSZ, as well as 3YSZ, undoped and doped samples was also calculated at a sintering temperature of 1400°C for one hour, as seen in Figure 23. The nickel doped samples reached a greater theoretical density than those that were undoped.

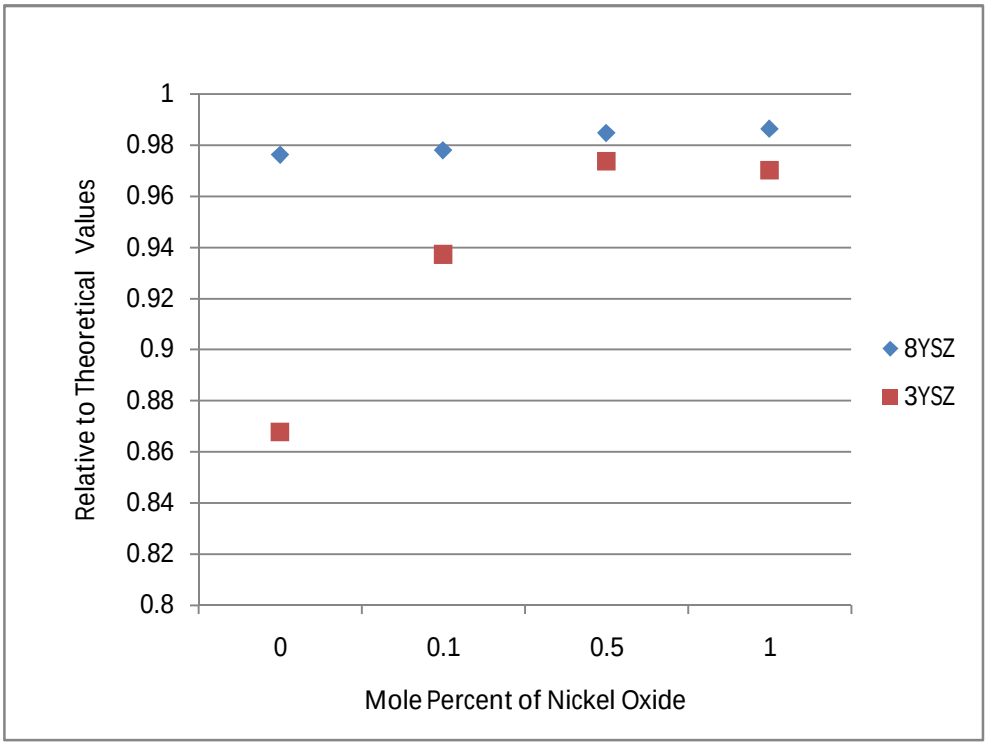

Figure 23. Relative Percent Density of YSZ Powders Sintered at 1400°C for One Hour.

Table 1 shows the correlation between all dopant levels used and the relative theoretical densities achieved for both 8YSZ and 3YSZ. As more nickel oxide is added, the density of the samples increases. Trace amounts are to be used to enhance the sintering performance without decreasing the ionic conductivity. The trend indicated by the pressed pellet densities indicate that the difference between the 0.5 and 1mol% is minimal and additions beyond 1mol% may not yield any advantage.

Table 1. % Theoretical Density of 8YSZ and 3YSZ with Respect to Mol% of Nickel

% Theoretical Density for 1300°C for One Hour				
Mol% Nickel	0	0.1	0.5	1
8YSZ	79.49	84.1	95.3	95
3YSZ	67.6	80.5	92.7	96.7
% Theoretical Density for 1400° for One Hour				
Mol% Nickel	0	0.1	0.5	1
8YSZ	97.63	97.8	98.47	98.64
3YSZ	86.78	93.72	97.36	97.02

Dilatometer

The onset sinter temperatures of the samples are shown in Figure 24 below. Sintering onset occurred with lower temperatures as more nickel was added to the YSZ powders. The onset sintering temperature is found using the dilatometer graphs shown in Figure 25 and Figure 26. Where the slopes of the horizontal line and the vertical line intersect is the onset temperature, according to the dilatometry data shown in Figure 25. Both 8YSZ and 3YSZ samples with nickel concentrations of 0, 0.1, 0.5, and 1 mole percent were examined. Higher quantities of nickel dopant resulted in lower onset temperatures for sintering. Comparison of nickel concentration versus maximum percent of relative shrinkage in µm is shown in Table 2. Shrinkage improves greatly with nickel concentration. 8YSZ has a shrinkage increase of 43.57% when comparing one mole percent Ni-8YSZ to 8YSZ. Similar results, as indicated in Table 2 for 3YSZ, have a 135.85% increase in shrinkage for one mole percent over the baseline sample.

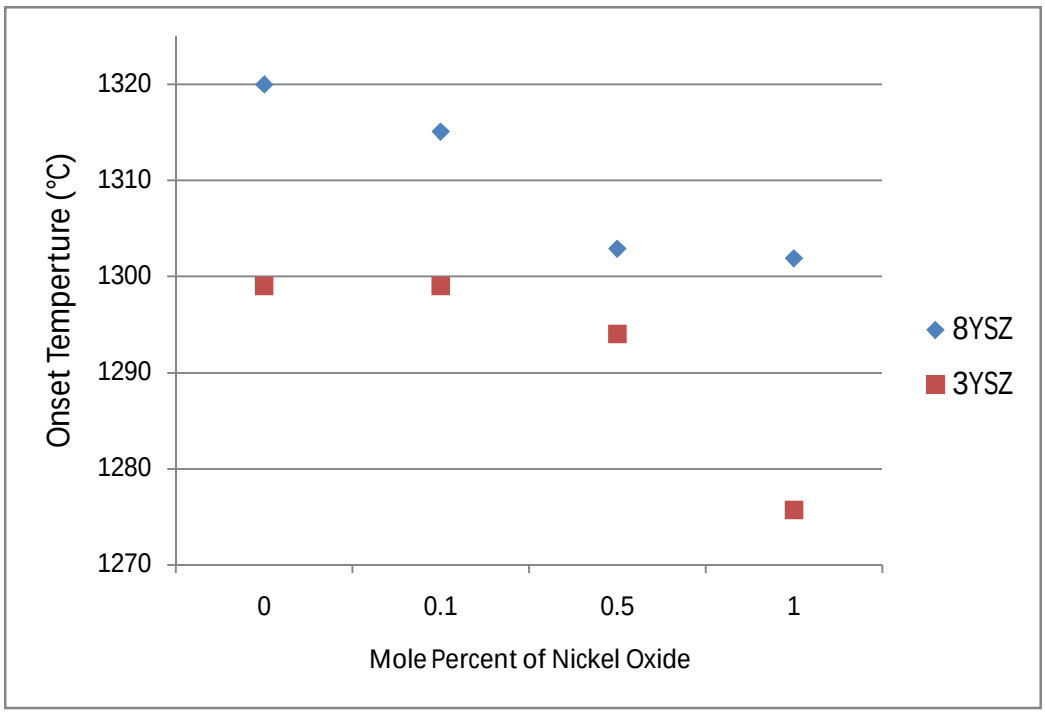

Figure 24. Onset Temperatures for Sintering

Table 2. Percent of Electrolyte Relative Shrinkage

Percent of Relative Electrolyte Shrinkage				
Mol% Nickel	0	0.1	0.5	1
8YSZ	14.34	17.94	19.64	20.04
3YSZ	8.41	14.64	19.22	19.78

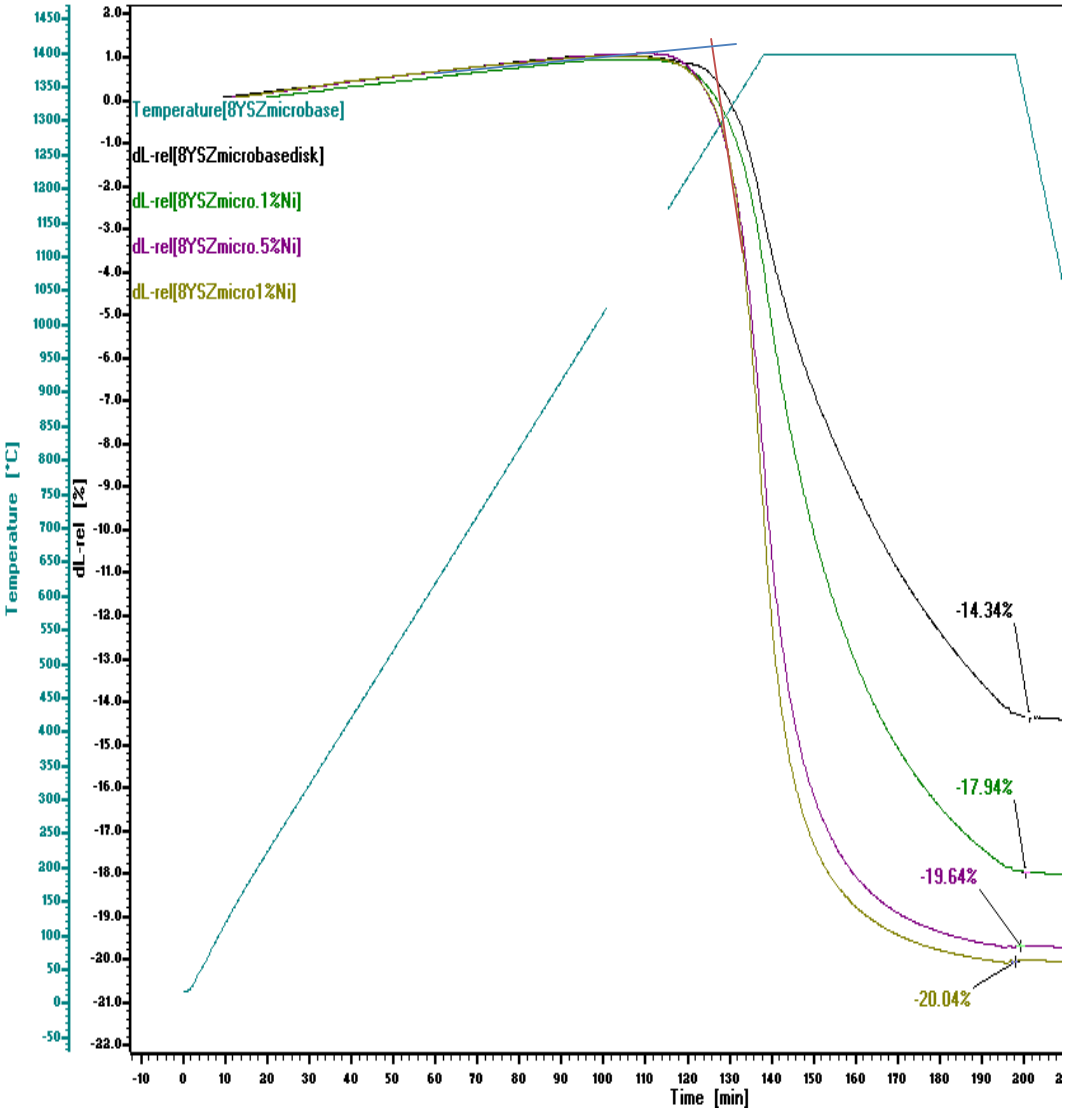

Figure 25. 8YSZ With Nickel Dopant Concentration on Dilatometer Chart

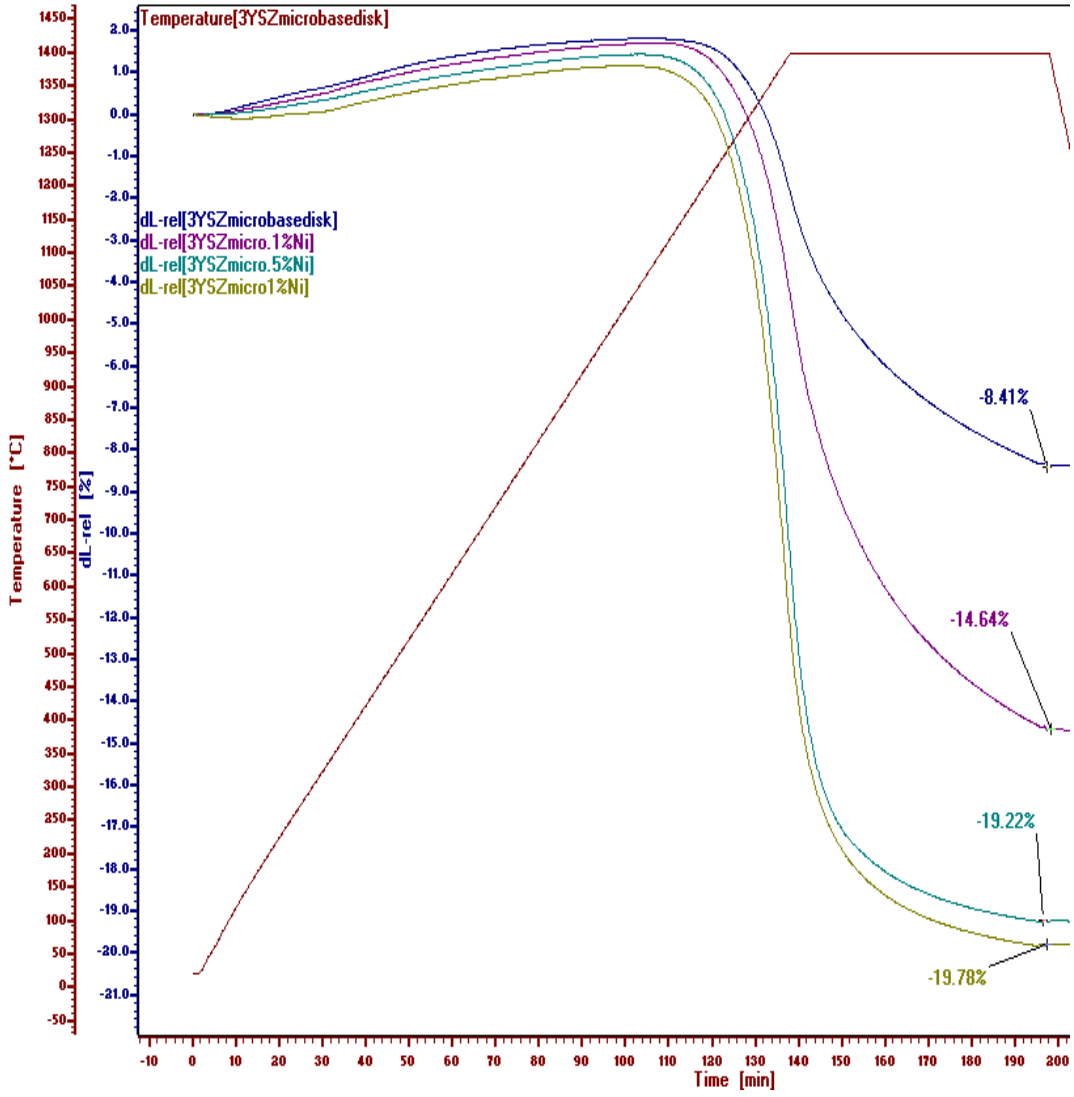

Figure 26. Dilatometry Analysis of 3YSZ Micro Powders

The maximum rate of sintering was also determined, in µm/min, from the time derivative of % change in length. The peak of the derivative was the highest rate of sintering that occurred during the test. One mole percent of NiO in YSZ was substantially higher than baseline YSZ. The sintering rates are shown for one mole percent of dopant for 8YSZ and 3YSZ in Figure 27 and Figure 28, respectively. The maximum sintering rate was found for each nickel dopant concentration and is shown in

Table 3 below. For each incremental step in nickel concentrations, the rate of sintering was higher for the amounts used in the experiment. The change in the 8YSZ sintering rate from baseline to one mole percent increased from 14.27µm/min to 39.4µm/min.

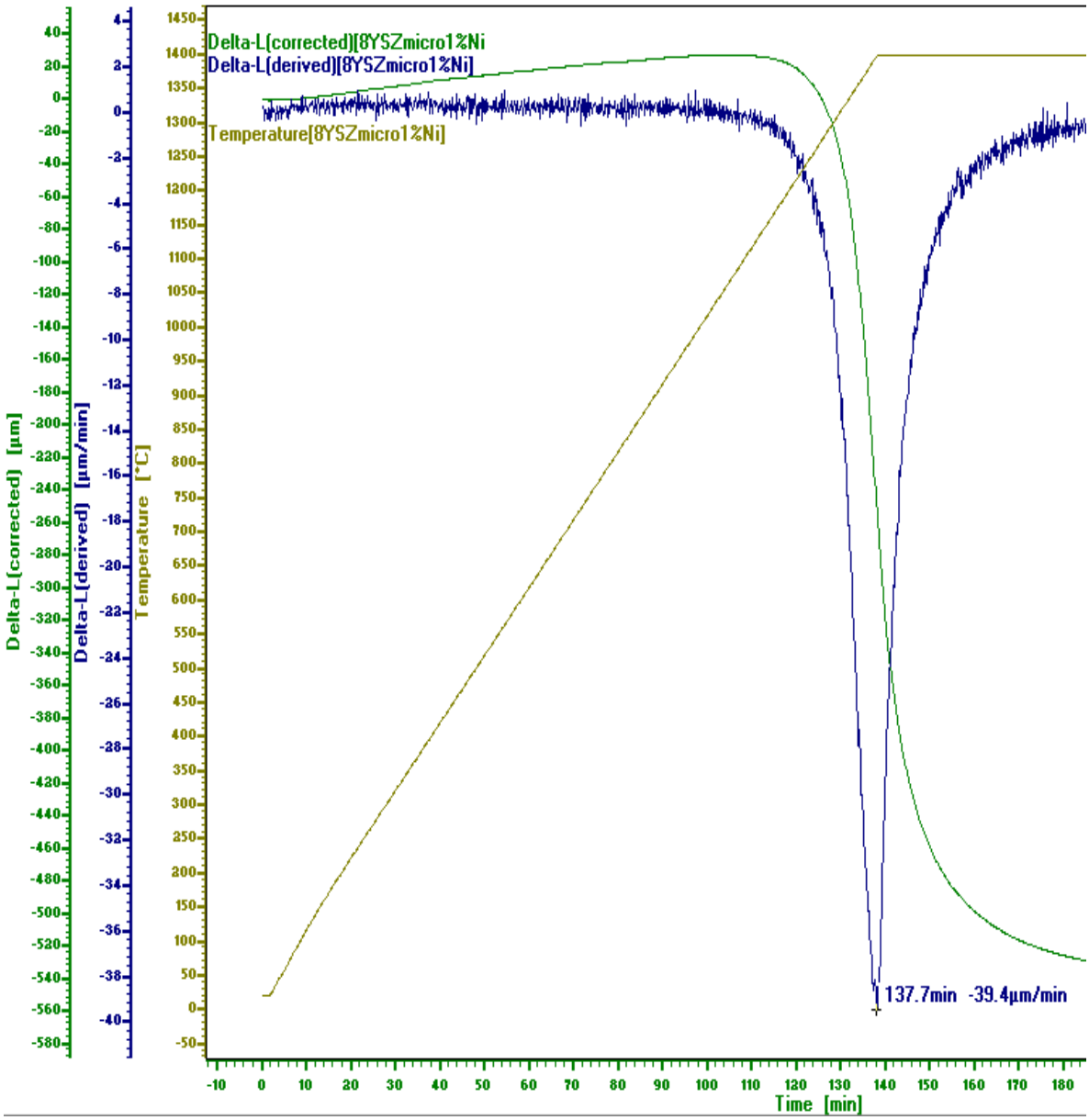

Figure 27. Sintering Rate (µm/min) for 1 Mol% Nickel Doped 8YSZ

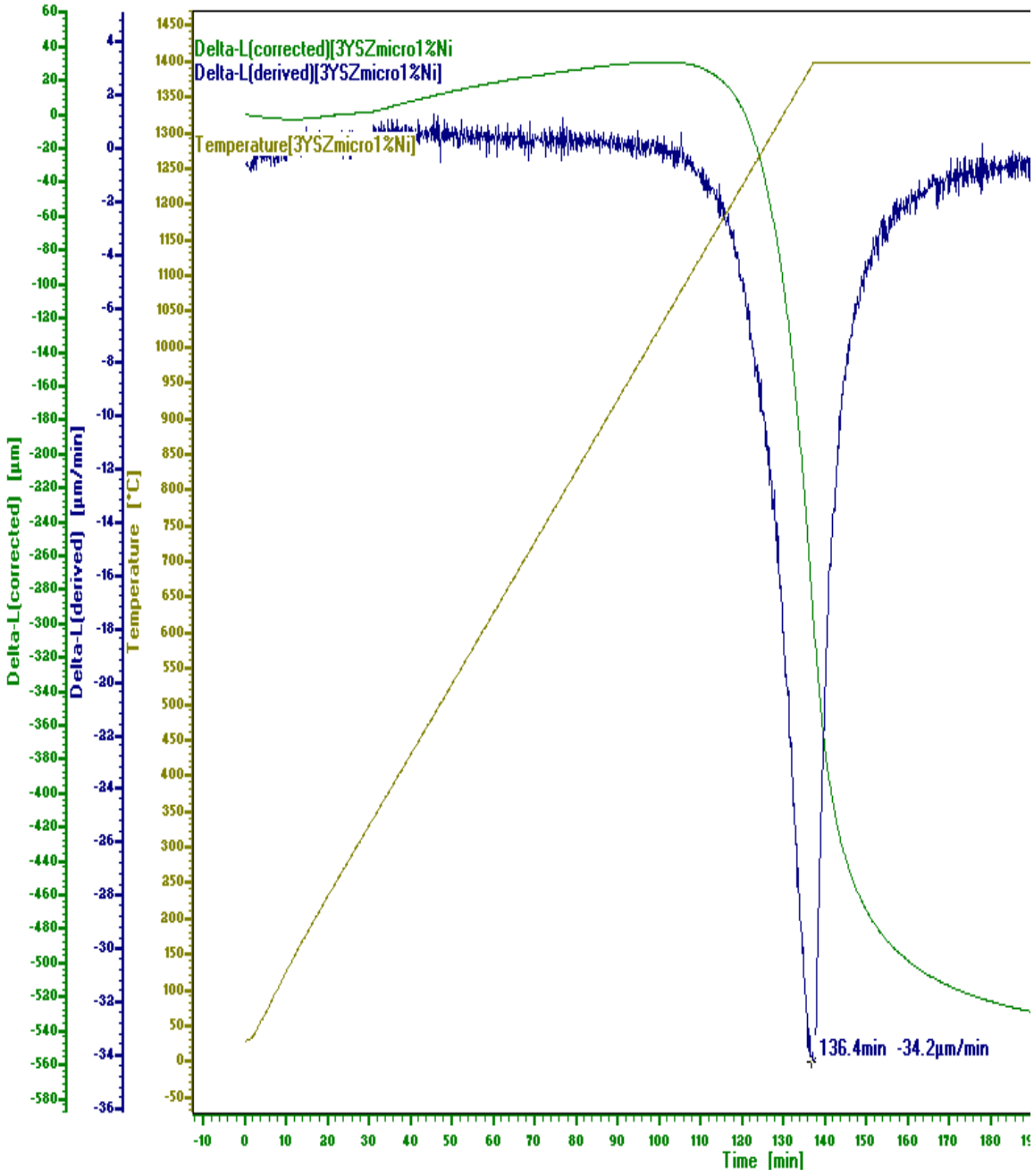

Figure 28. Sintering Rate (µm/min) for 1 Mol% Nickel Doped 3YSZ

Table 3. Maximum Sintering Rate (μm/min)

Maximum Sintering Rate (μm/min)				
Mol% Nickel	0	0.1	0.5	1
8YSZ	14.27	19.43	34.8	39.4
3YSZ	11.5	18.41	35.7	34.2

Dilatometry tests proved that sintering occurred at a lower temperature and sintering rate improved with a nickel dopant. Doped samples were denser by the end of the run. Observations indicate that the nickel oxide dopants also improved the surface diffusion of the electrolyte. More importantly, the bulk diffusion, responsible for density packing factor of the ceramic material, was optimized with the nickel oxide. The grain boundaries that were in contact grew together, causing a more dense mass.

Impedance Spectroscopy

Two measurements were recorded during the ionic conductivity test, grain boundary and the bulk conductivity of the YSZ. Total ionic conductivity can be found by adding the bulk and the grain boundary conductivities together. The transfer of the ions from the oxygen to the hydrogen side of the electrolyte must not be restricted by the nickel dopant. Baseline runs with the 8YSZ were used to compare the effects that the nickel oxide dopant with the YSZ would have in the conductivity test. 8YSZ, as well as nickel doped specimens, were sintered at 1400°C or 1300°C prior to conductivity testing. This was to determine the effects of temperature and nickel dopant on the ceramic material.

Only the highest concentration of NiO in YSZ was tested because it was determined that concentrations with less than one mole percent would not impact the conductivity. The comparison of the total ionic conductivity for 1400°C and 1300°C sintered samples is shown in Figure 29 and Figure 30, respectively. The high sintering temperature comparison shows the doped samples are slightly under the baseline runs. The change is small enough to state the nickel oxide dopant is comparable to plain 8YSZ.

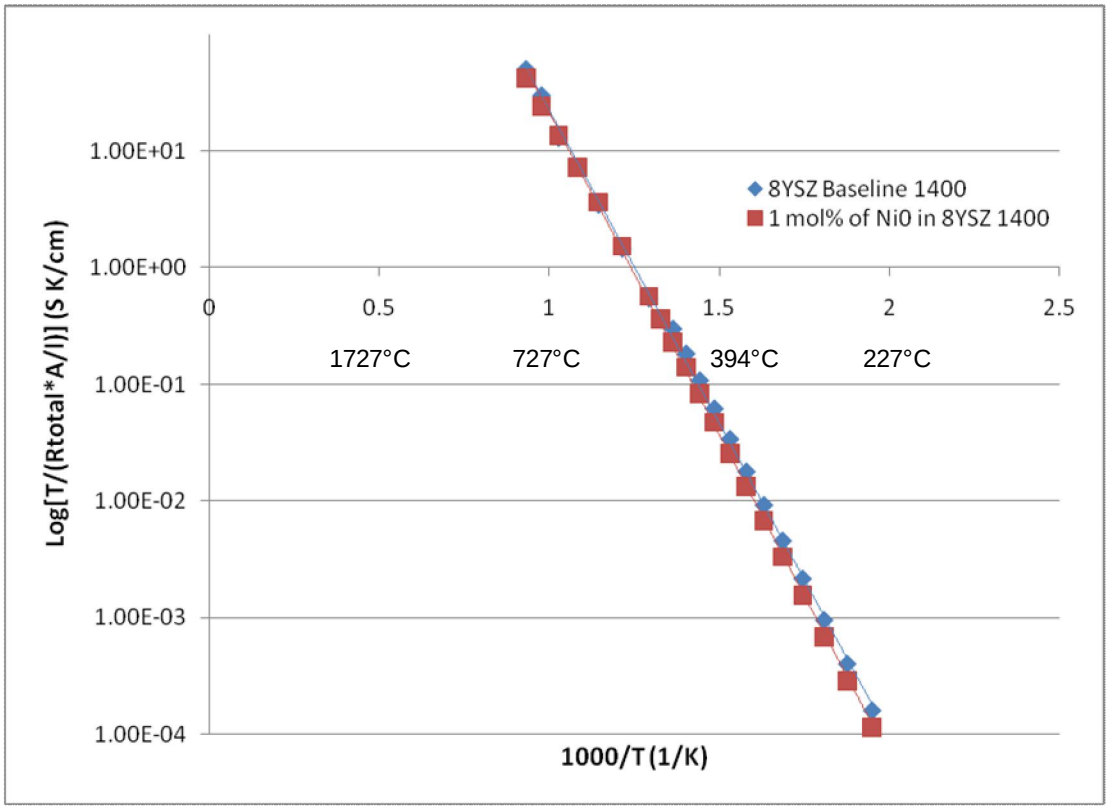

Figure 29. Total Conductivity for 8YSZ Sintered at 1400C for One Hour

Lower sintering temperature runs indicate the doped samples have higher ionic conductivity. For lower sintering temperatures, the density of the electrolyte is improved as well as the ionic conductivity with the addition of one mole percent of nickel oxide. The test indicates that the nickel dopant does not cause degradation to the conductivity.

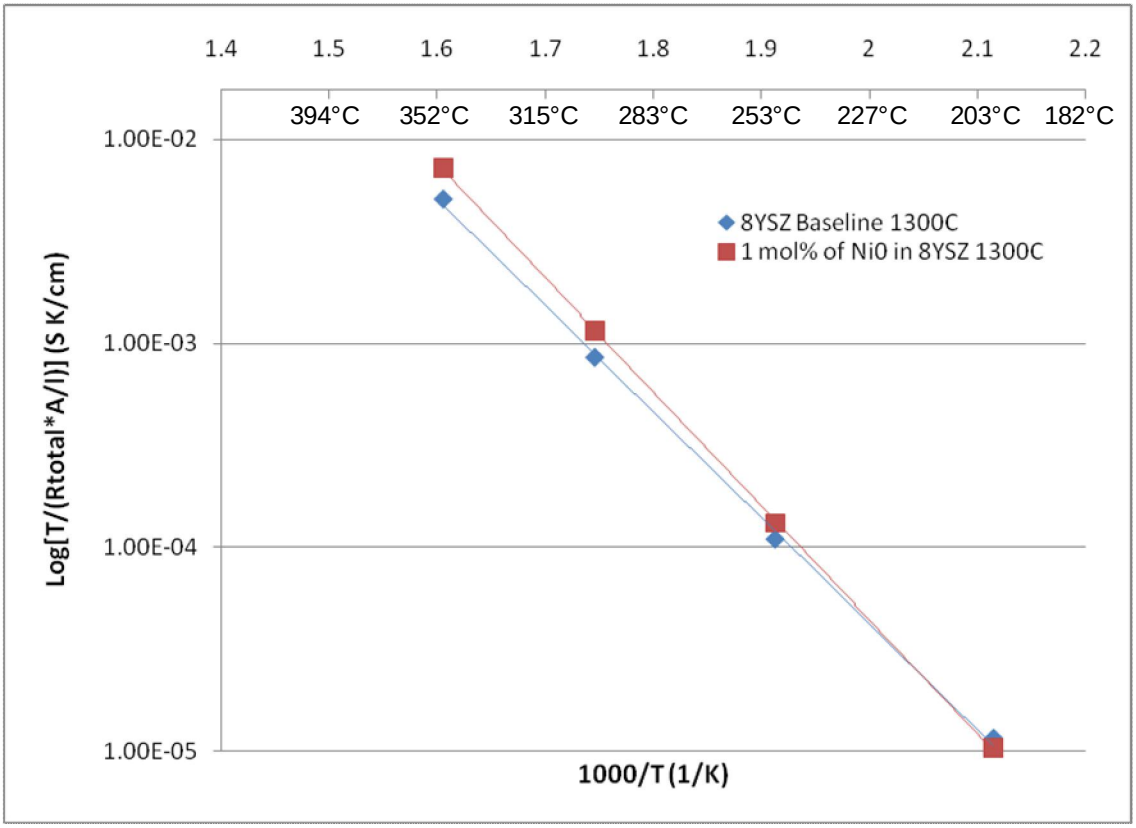

Figure 30. Total Conductivity for 8YSZ Sintered at 1300C for One Hour

A closer look at the grain boundaries and bulk conductivities of the samples was also conducted. The grain boundary results shown in Figure 31 appear to have no discernable difference between the doped and undoped samples at 1400°C. However, with a sintering temperature of 1300°C, the ionic conductivity at the grain boundaries of the sample is higher. The resistance at the grain boundaries when using the low temperature setting is reduced with the addition of nickel.

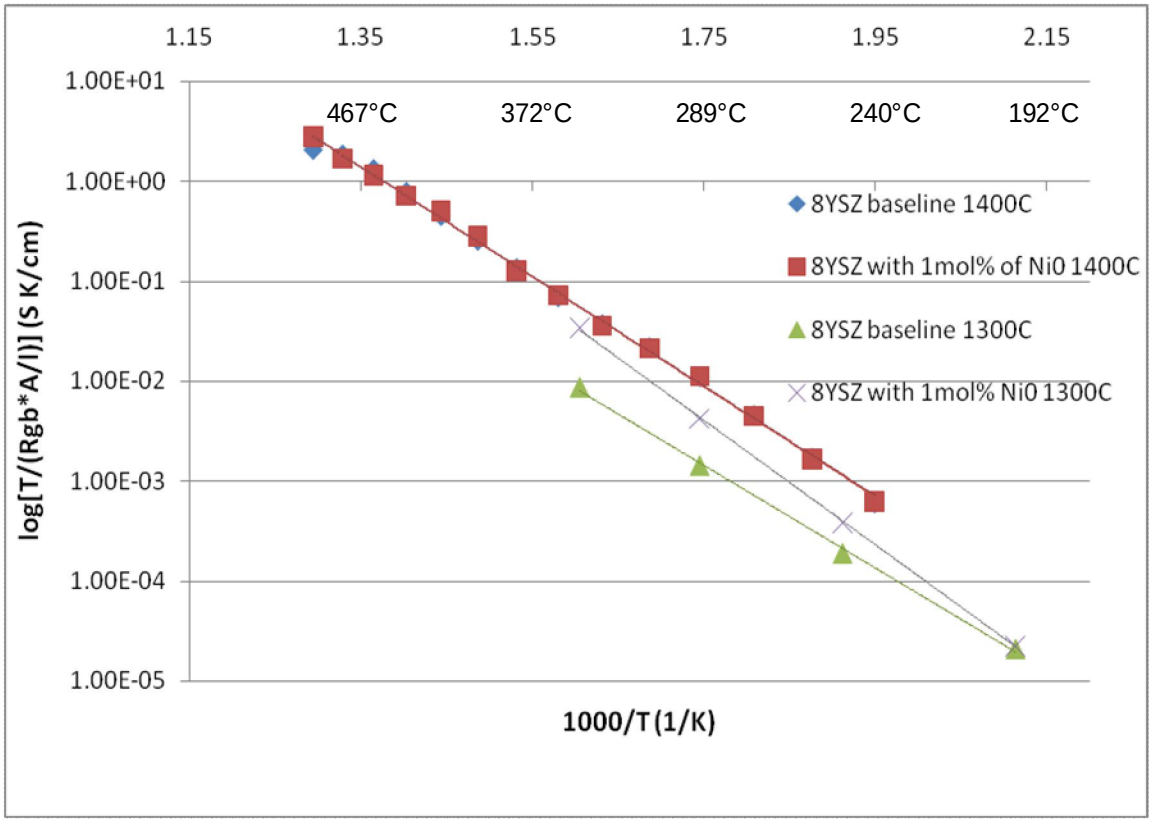

Figure 31. Grain Boundary Ionic Conductivity of 8YSZ

Bulk ionic conductivity is the conductivity over the entire surface area of the sample. The high sintering temperature for bulk conductivity has minimal difference between the doped and undoped samples, as shown if Figure 32. Undoped 8YSZ has a slightly higher conductivity at certain temperature ranges. Bulk conductivity at high temperature demonstrates that the dopant does not compromise the conductivity of the sample.

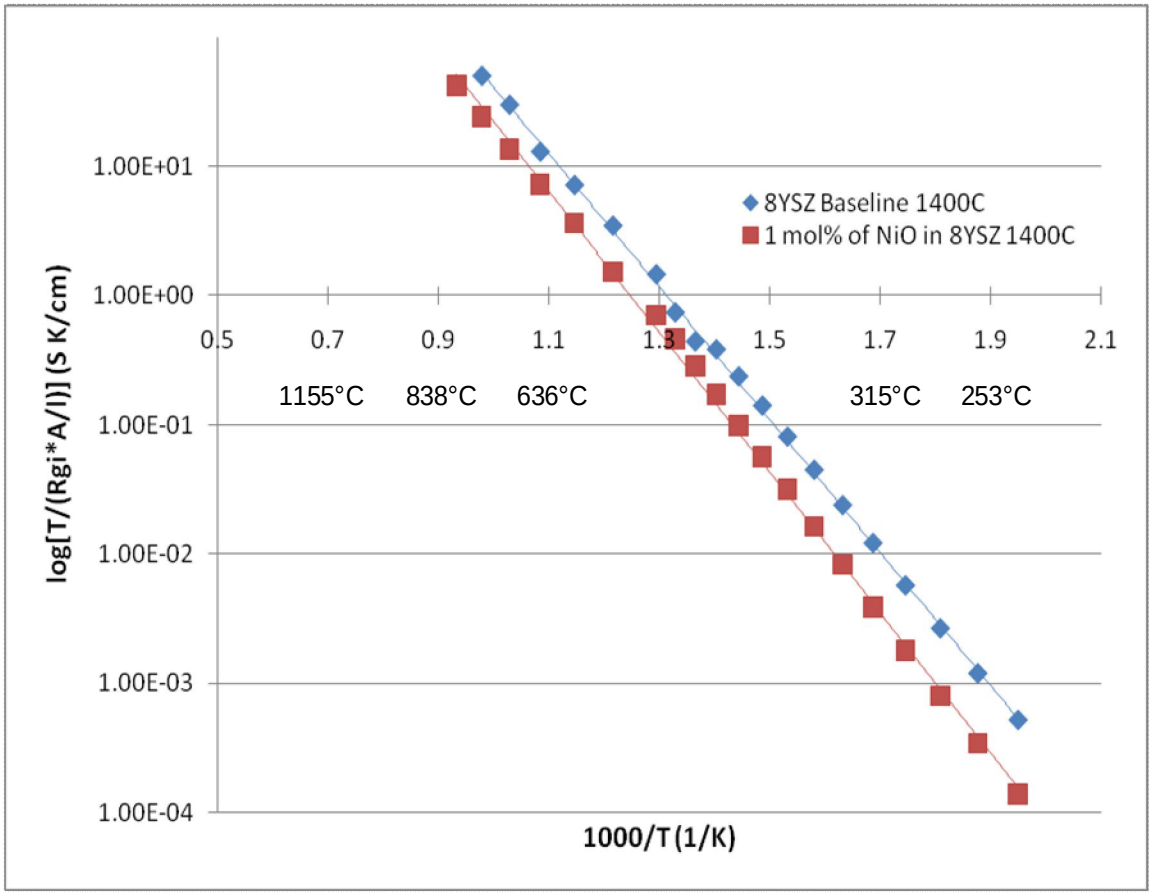

Figure 32. Bulk Ionic Conductivity for 8YSZ Sintered at 1400 for One Hour

Doped samples that were sintered at 1300°C for one hour also had bulk conductivities slightly lower than undoped samples, as shown in Figure 33. Bulk conductivity showed a slight decrease at both sintering temperatures. However, the grain boundary conductivity increases as sinter temperature is lowered, suggesting that the nickel oxide resides in the grain boundaries of the host YSZ powders. Imperfections could be caused by the nickel oxide at the grain boundary locations causing the ionic conductivity to actually increase with nickel dopant presence. Nickel oxide can be used as a dopant for improved sintering performance with negligible effects on the ionic conductivity of the electrolyte.

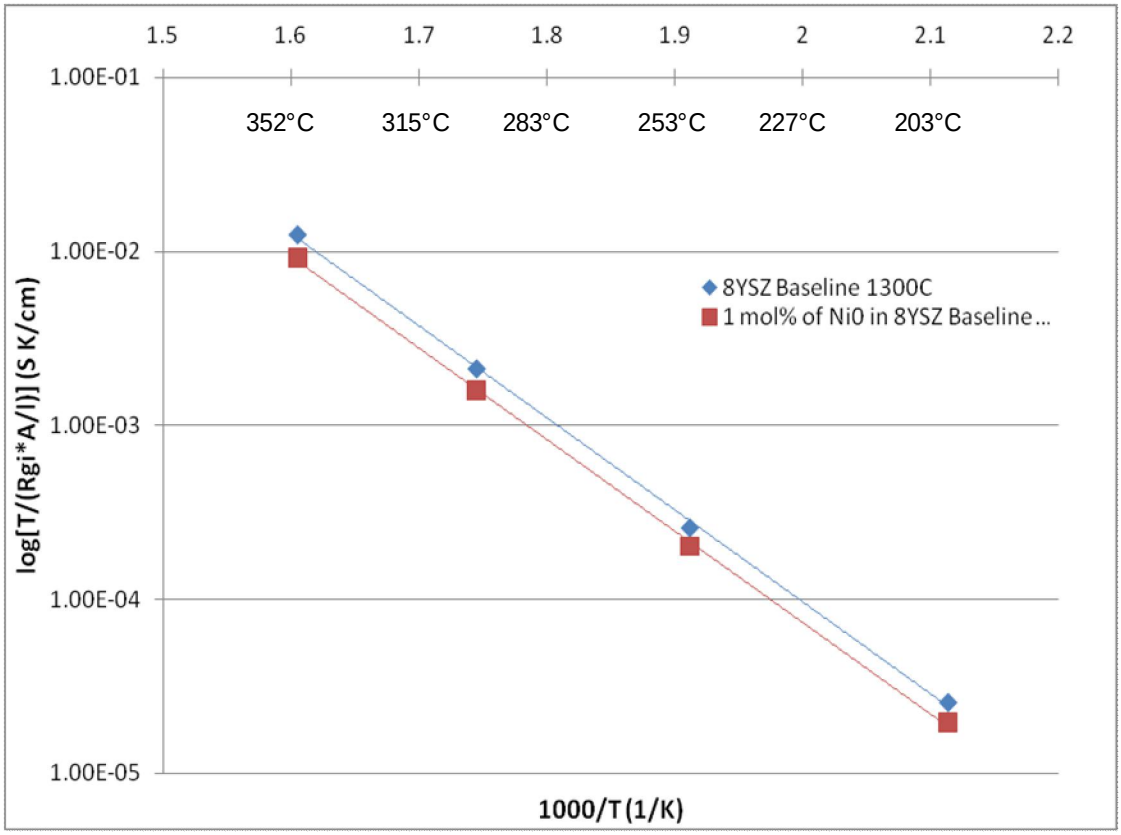

Figure 33. Bulk Ionic Conductivity for 8YSZ Sintered at 1300 for One Hour

Centrifugal Speed

Pressed pellets were used for preliminary test involving the percent theoretical density, dilatometry, and electrochemical impedance spectroscopy test. The upcoming tests were conducted to optimize the tape slurry recipe. A base test was performed with the centrifugal mixer to test the revolutions per minute for a five minute cycle necessary to homogenize the slurry. In Figure 34, from left to right as shown, the rpm is 2000, 1500, 1000, and 500 each run for five minutes. After an undisturbed period of five days, the samples were visually inspected to determine the optimum rpm. The 1500 rpm test (second sample from the left) has the most desirable particle suspension. The top of the

vial was still cloudy which indicates that suspended particles are still in the solution. An ideal level of dispersion is the minimal possible amount of 2% level. The mechanical mixing process was adequate enough to break the VDW bonds resulting in adequate coating of the particles.

Figure 34. Centrifugal Speed Test with 8YSZ Slurry

Dispersion Study

The dispersion of the particles in the slurry had to be determined when utilizing the centrifugal mixer as well. The first of the dispersion tests was conducted with a mixture of 8YSZ, xylene/ethanol, and MFO dispersant at increments ranging from 1-5%. A visual comparison such that of Figure 35, showed high levels of sedimentation in the 1% doped sample (on the left). None of the samples displayed differences in

sedimentation and solution clarity at the top. However, noticeable difference was observed at the bottom between the 2 and 3% samples with similar sediment levels but dissimilar transparency.

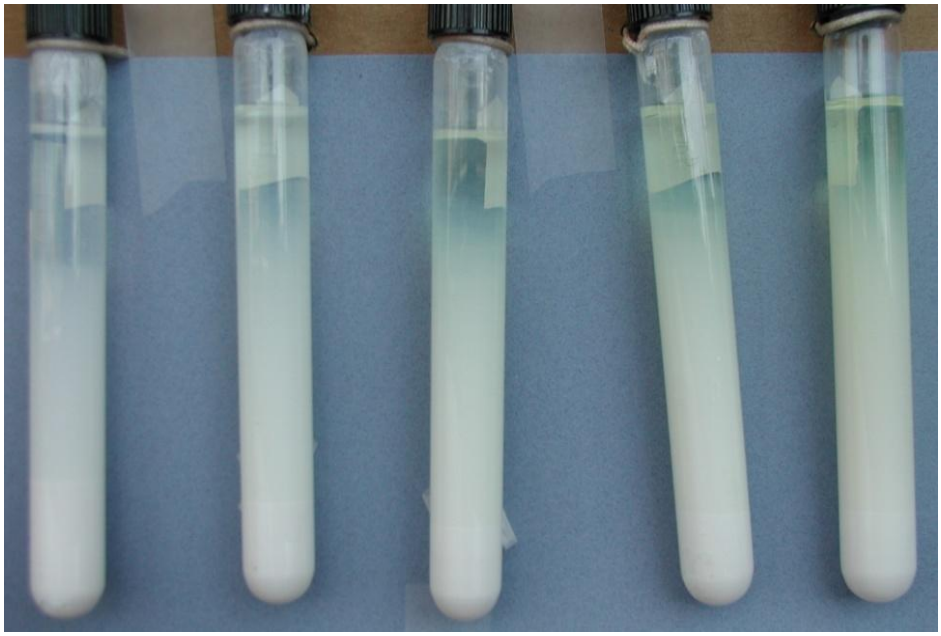

Figure 35. Centrifugal Test With 1-5% of MFO in 8YSZ in 1% increments (From Left to Right)

Nickel oxide mixed with MFO was the last sediment study. A solution of nickel oxide and xylene/ethanol was mixed with 1-5% increments of MFO dispersant. Results were similar to YSZ study for the nickel powder with 1% dispersant; the particles settled quickly. Little particle settling occurred with the 4-5% range, while a balance of transparency and sedimentation was observed in 2-3% shown in Figure 36.

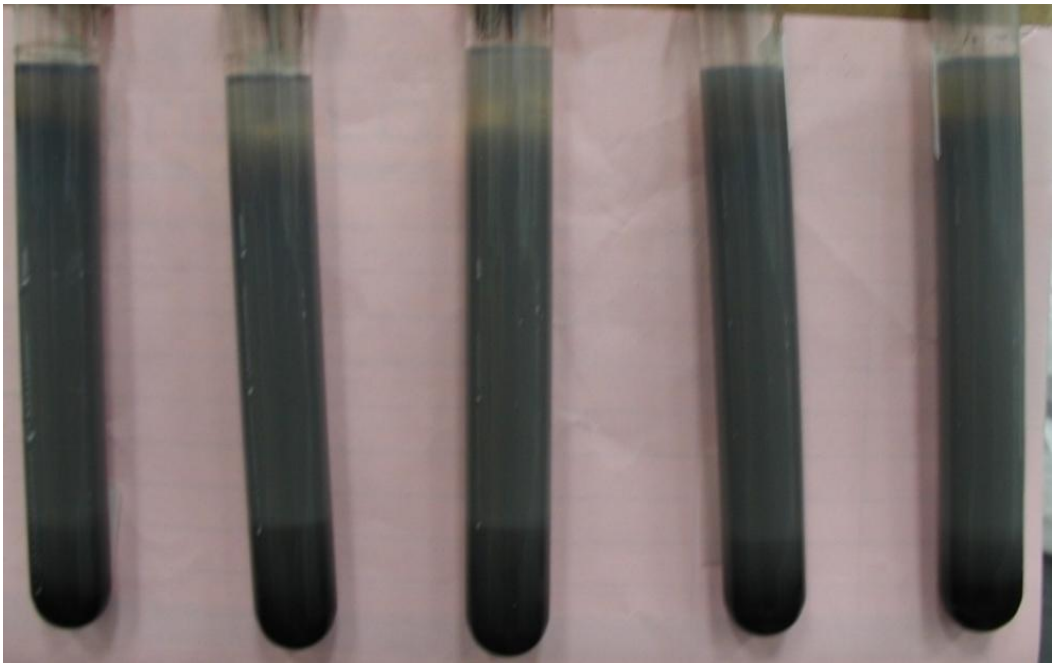

Figure 36. Centrifugal Test Nickel Oxide with 1-5% MFO in 1% increments (From Left to Right)

Nickel oxide and YSZ display good tape casting characteristics with the MFO weight percent in the 2-3% range. The particle dispersion in the 2-3% range of MFO displayed the ideal characteristics for both nickel oxide and YSZ. An ideal sample should have a small level of clarity at the top with densely packed sediment at the bottom. In the tape casting process, during the mixing of the nickel oxide and YSZ, the fish oil was added at 2.26 weight percent. This exact value was obtained from previous lab research. (64)

Density Study

Geometric density was found using Equation 2 for select samples cut from varying tape recipes. The density data was compared to the slurry recipe and tape casting process. A correlation of the process and slurry makeup was used to distinguish the

mechanism for the higher density samples. Displayed in Table 4 are the average densities of the nickel doped and plain YSZ samples. Both green and sintered densities were calculated in an attempt to correlate the progressive refining of the tape casting process with achieving higher densities. In Table 4 the anomaly of the green tape density being larger than the sintered density for 3YSZ at 1300°C is from a power failure in the lab during the sintering run. The electrolyte did not receive ample time to densify and thus having a lower density.

Table 4. Average Geometric Tape Densities

Average Green Tape Density (g/cm^3)				
	8YSZ	Ni-8YSZ	3YSZ	Ni-3YSZ
1400°C	2.61	2.60	2.89	2.74
1300°C	2.73	2.63	2.81	2.58
Average Sintered Tape Density (g/cm^3)				
	8YSZ	Ni-8YSZ	3YSZ	Ni-3YSZ
1400°C	3.81	3.99	3.44	4.04
1300°C	3.18	3.66	2.79	3.52

A total of 58 tape samples were used to calculate the percent of average density increase that the nickel doped samples had over YSZ samples. This average increased as well as the standard deviation of all of the tested sintered specimens are shown in Table 5 and Table 6. The nickel doped YSZ showed an increase in density over plain YSZ for both of the sintering cycles tested. There was minimal change in the standard deviation of the samples.

Table 5. Average Percent Increase in Density of Doped and Undoped YSZ

	YSZ	NiO YSZ	% Increase
1400°C			
8YSZ	3.81	3.99	4.51
3YSZ	3.44	4.04	14.85
1300°C			
8YSZ	3.18	3.66	13.11
3YSZ	2.79	3.52	20.74

Table 6. Standard Deviation of Sintered Doped and Undoped YSZ

Sinter Cycle	8YSZ	Ni-8YSZ	3YSZ	Ni-3YSZ
1400°C	0.45	0.22	0.28	0.37
1300°C	0.63	0.47	0.35	0.44

The test suggests that the minute changes in pouring of the slurry during the tape casting process did not affect the tape densities. The iterations in the tape casting process did not improve the tape densities tremendously but the quality of the tapes improved dramatically. Through processing iterations the smoothness and thickness of the electrolyte tape improved to SOFC quality. Pin holes first plagued the tape cast rendering the tape useless for gas separation. A heating period of the slurry prior to tape casting virtually eliminated the pinholes.

Densities of the sintered tapes were lower than that of the sintered pressed pellets; particle packing factor is greater in pressed pellets than in tape casting. The amount of organics needed for a functional tape slurry limits the amount of particle packing. Finer powders and additional process refinement could help in achieving higher tape densities.

Concentric Ring on Ring

Eighteen samples were taken from each tape recipe and sintered at three distinct temperature ranges. Doped and undoped samples were compared to determine the percent increase in flexural strength (MPa). The mass of the load ring was added to the static mass and the flexural strength was found, which was used in Equation 4. A total of 216 samples were tested. In every case, the doped samples had higher fracture strength, as shown in Figure 39 through Figure 39. Any samples with edge propagated fractures were discarded for an accurate measure of strength.

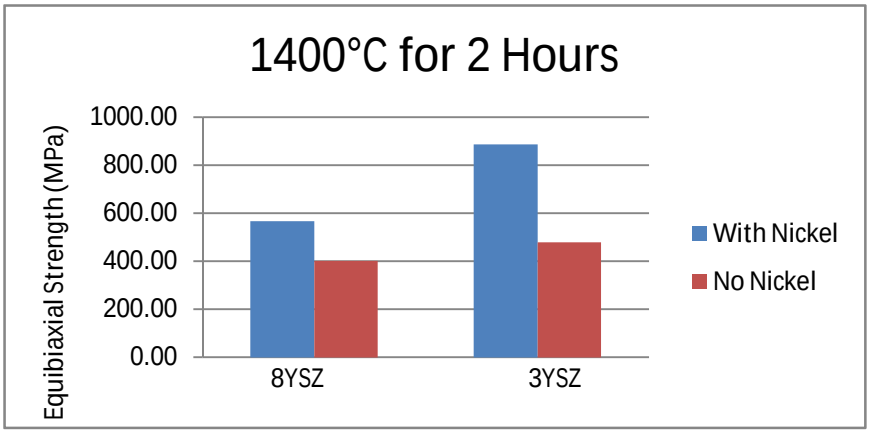

Figure 37. Equibiaxial Strength of Ni-YSZ and YSZ Tapes at 1400C

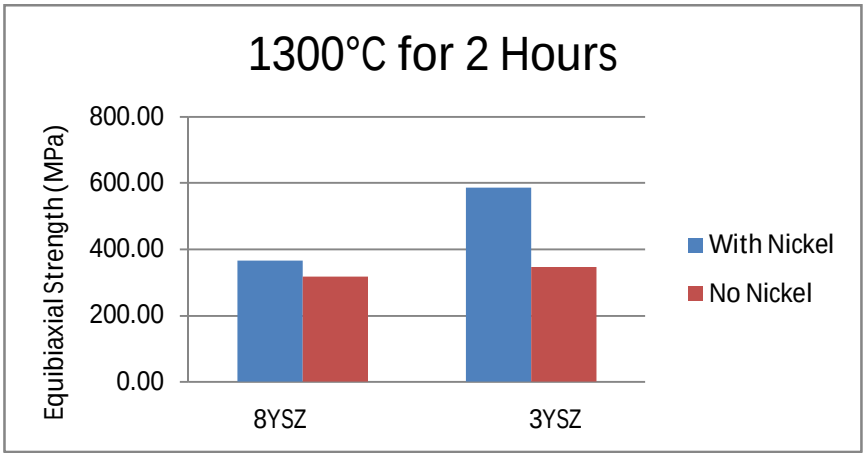

Figure 38. Equibiaxial Strength of Ni-YSZ and YSZ Tapes at 1300C

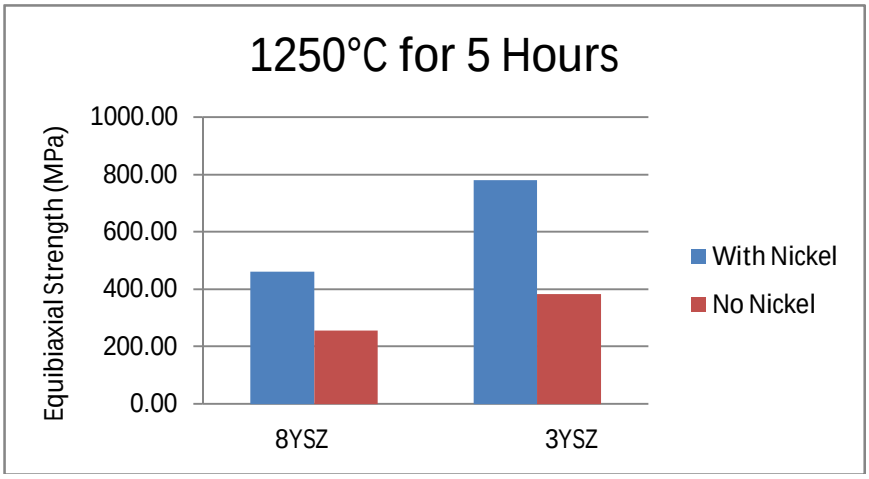

Figure 39. Equibiaxial Strength of Ni-YSZ and YSZ Tapes at 1250C

Averages of the uniaxial test were taken to compare the doped tapes to the plain YSZ tapes. The lowest percent increase of the equibiaxial strength was 13.59% while the greatest improvement was 50.91%. Table 7 shows the comparison of the averages of the sinter taped strength.

Table 7. Doped and Undoped YSZ Average Equibiaxial Strength Comparison

	Doped	Undoped	% Increase
1400°C For 2 Hours			
8YSZ Strength (MPa)	566.56	401.94	29.06
3YSZ Strength (MPa)	886.55	478.35	46.04
1300°C For 2 Hours			
8YSZ Strength (MPa)	365.99	316.55	13.51
3YSZ Strength (MPa)	586.09	346.04	40.96
1250°C For 5 Hours			
8YSZ Strength (MPa)	461.15	255.76	44.54
3YSZ Strength (MPa)	778.77	382.27	50.91

Differing fracture strengths were likely due to internal cracks in the electrolyte. Premature failure could also result from the sintered samples not being completely flat. Edge ripples did form from the sintering process with some samples. Ripples are areas that have higher stress concentration, causing failure at values lower than the actual sample's strength. To reduce the error in this process, multiple samples were tested to acquire a large data base for comparison.

All of the cases shown in Figure 40 through Figure 43 displayed a trend of increased strength as the testing progressed. They were all tested in chronological order. The data suggest that the tape casting recipe and process was refined as the testing continued. Nickel doped samples achieved higher equibiaxial strength than the undoped samples.

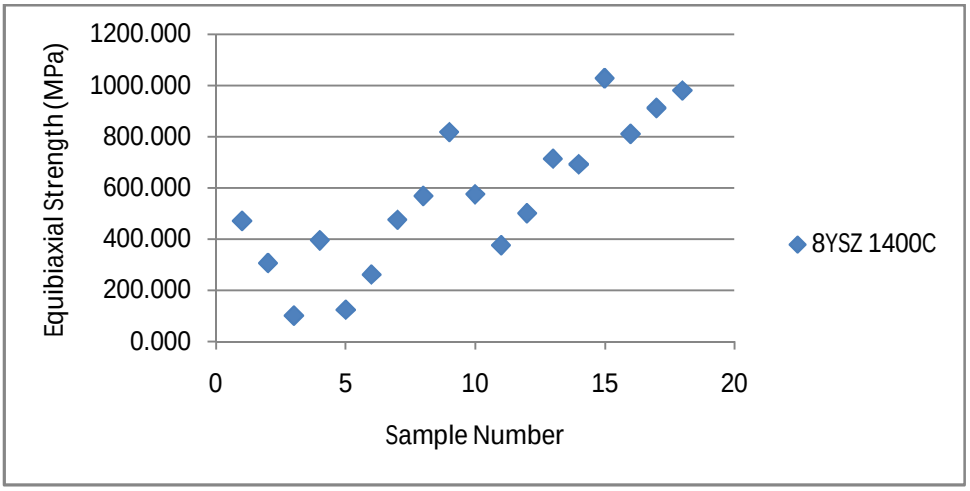

Figure 40. Equibiaxial Strength of 8YSZ Sintered at 1400°C

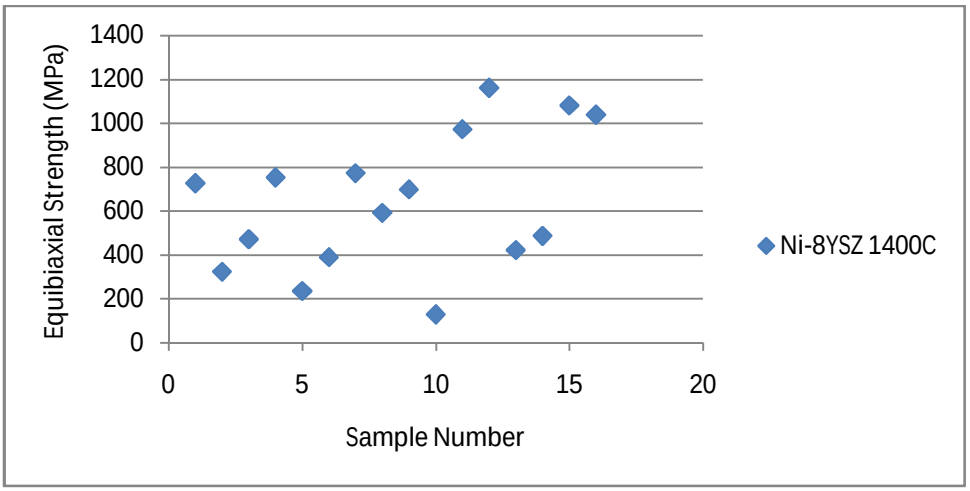

Figure 41. Equibiaxial Strength of Ni-8YSZ Sintered at 1400°C

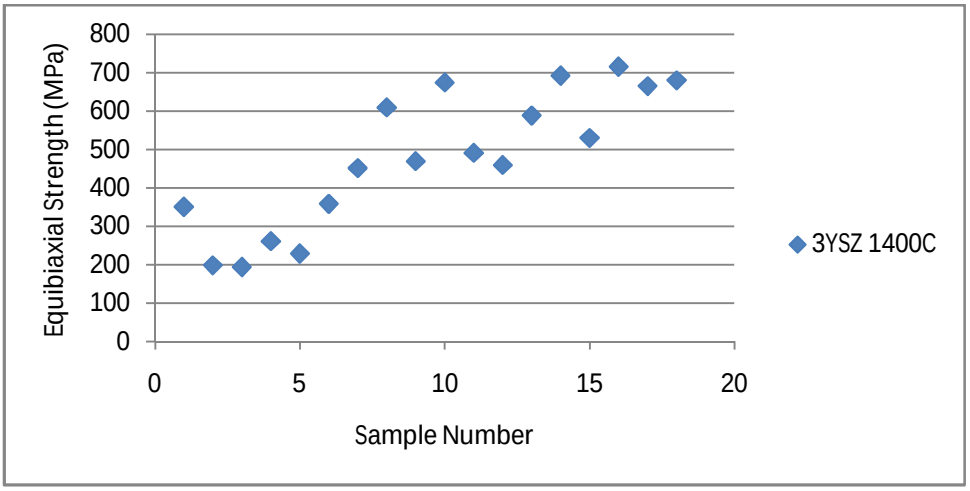

Figure 42. Equibiaxial Strength of 3YSZ Sintered at 1400°C

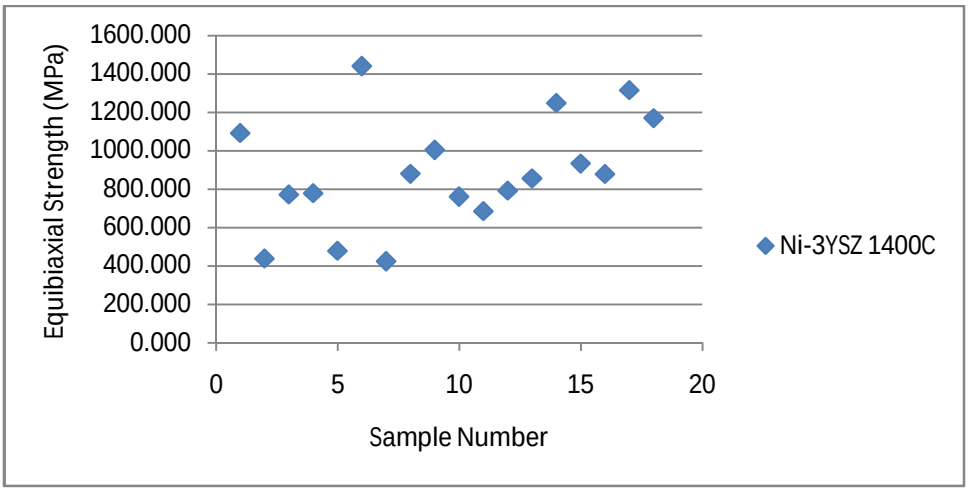

Figure 43. Equibiaxial Strength of Ni-3YSZ Sintered at 1400°C

Only the 8YSZ samples showed the chronologically increasing strength trend. The other tape recipes showed a linear trend with stochastic outliers when sintered at 1300°C. Another example of doped samples having a clear strength improvement over undoped is shown in Figure 44 through Figure 47.

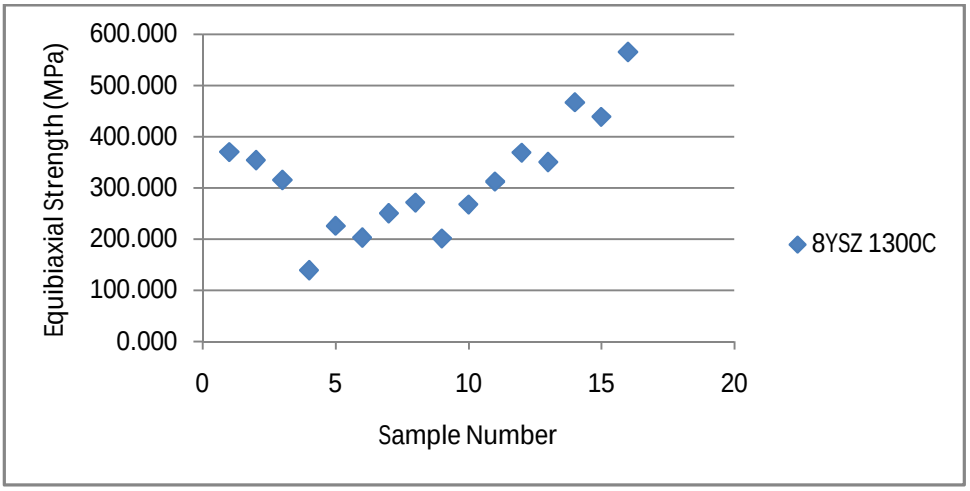

Figure 44. Equibiaxial Strength of 8YSZ Sintered at 1300°C

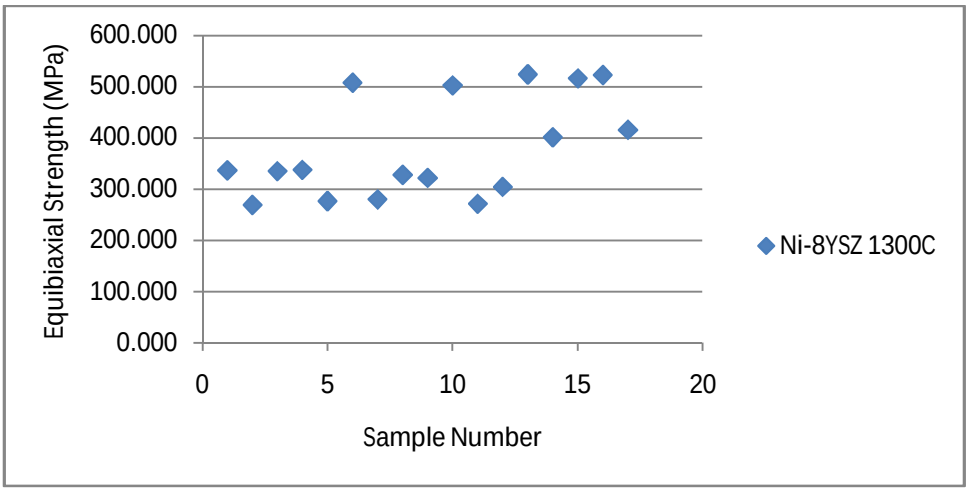

Figure 45. Equibiaxial Strength of Ni-8YSZ Sintered at 1300°C

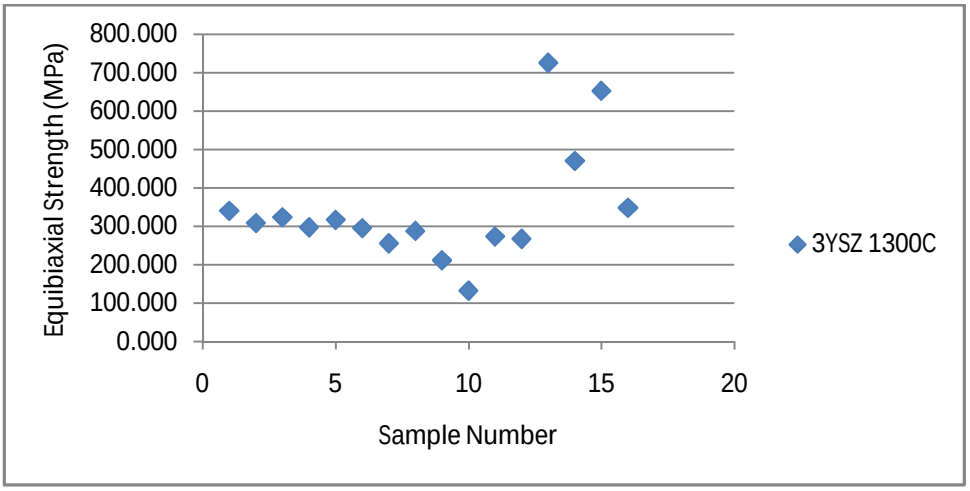

Figure 46. Equibiaxial Strength of 3YSZ Sintered at 1300°C

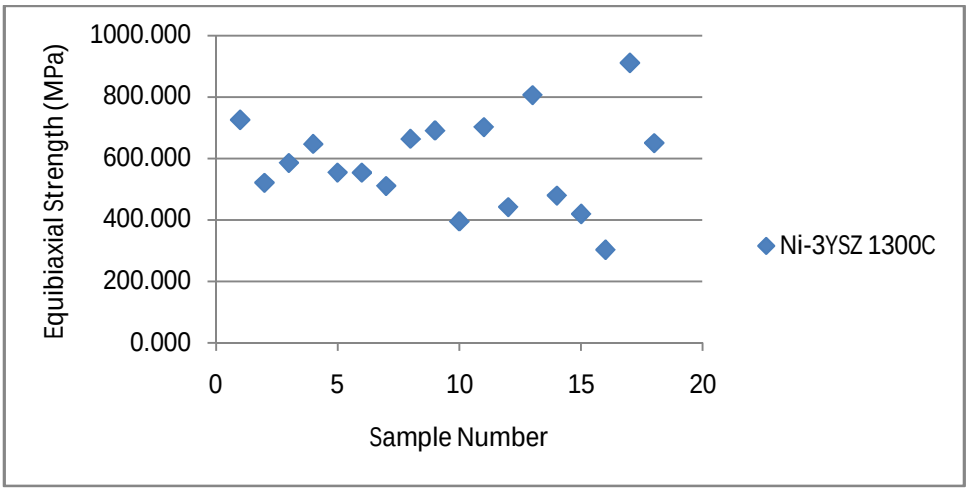

Figure 47. Equibiaxial Strength of Ni-3YSZ Sintered at 1300°C

Random outliers show up in the linear trends from the recipes sintered at 1250°C shown in Figure 48 through Figure 51. An increase was not experienced as the testing continued; however, the doped electrolyte did reach higher strength values than undoped electrolytes as expected. The sinter cycle at 1400°C was the only cycle that showed an increasing trend as the process and recipes were refined. The other two cycles had constant linear trends with random outliers. Averages were taken for the four different tape casting recipes sintered at three distinct sintering cycles to obtain approximate values

for strength. In Table 8 the standard deviation of the samples tested was calculated for each recipe at the three different sintering temperatures.

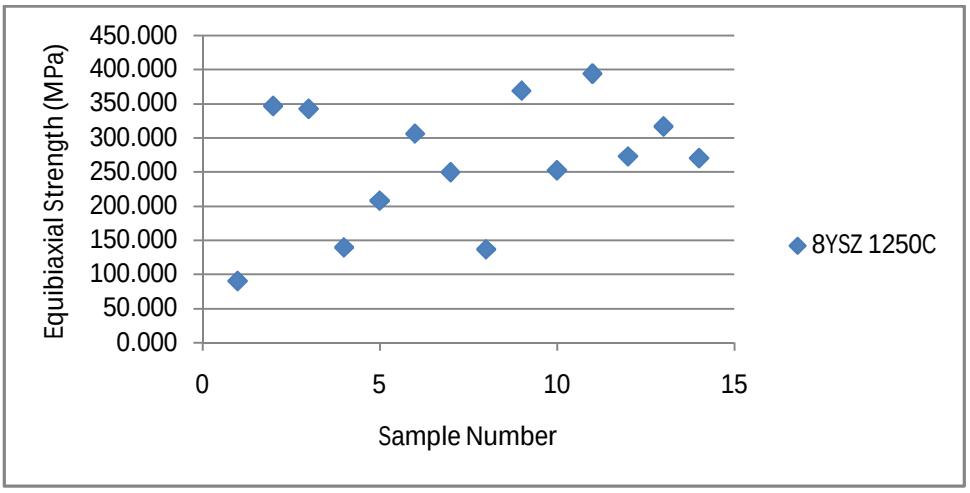

Figure 48. Equibiaxial Strength of 8YSZ Sintered at 1250°C

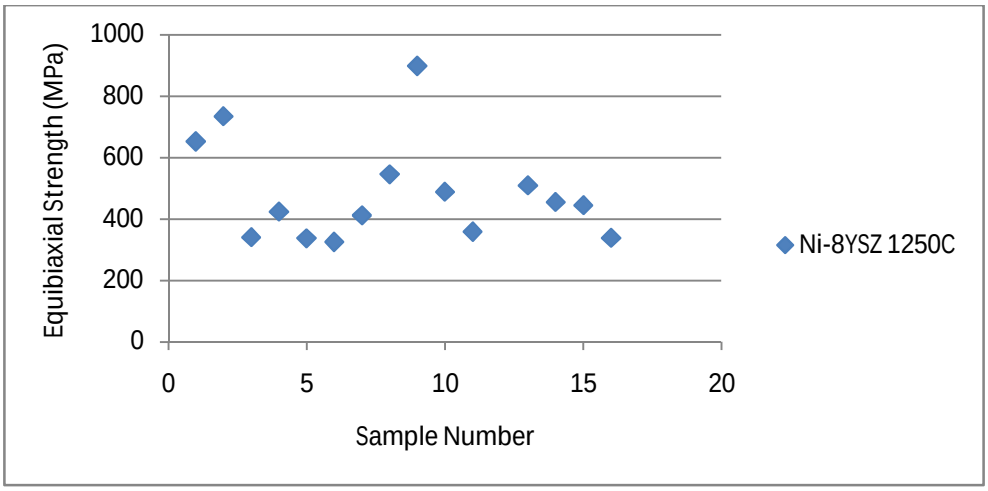

Figure 49. Equibiaxial Strength of Ni-8YSZ Sintered at 1250°C

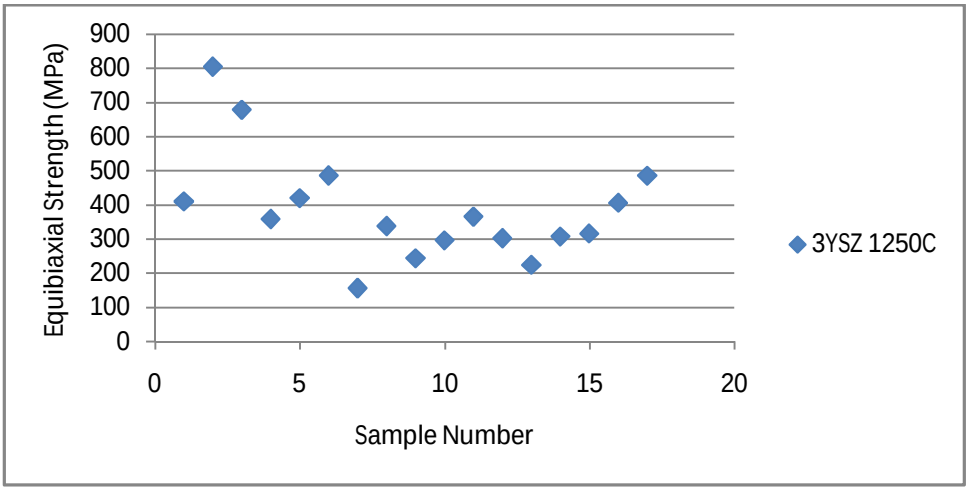

Figure 50. Equibiaxial Strength of 3YSZ Sintered at 1250°C

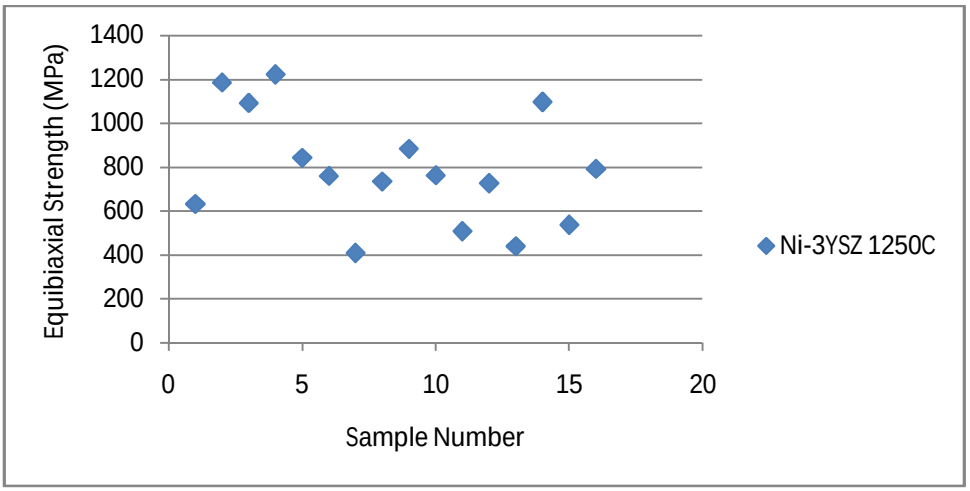

Figure 51. Equibiaxial Strength of Ni-3YSZ Sintered at 1250°C

Table 8. Standard Deviation of All YSZ Equibiaxial Strength Testing at Different Sintering Cycles

Sintering Cycle	8YSZ	Ni-8YSZ	3YSZ	Ni-3YSZ
1400°C For 2 Hours	278.89	312.71	179.64	290.23
1300°C For 2 Hours	110.29	98.22	151.98	153.51
1250°C For 5 Hours	92.12	165.03	160.56	256.42

Microstructures

The nickel doped tapes had larger grains than undoped samples, as displayed in Figure 52 and Figure 53 when sintered at 1400°C. Grain size, from Figure 52, for the 8YSZ and Ni-8YSZ is 0.74µm and 1.18µm, respectively, while the 3YSZ and Ni-3YSZ grain size, from Figure 53, was determined to be 0.38µm and 0.61µm, respectively. The low magnification in the nickel doped 8YSZ shows a large surface of smooth dense electrolyte which is unique from all the other low magnification micrographs.

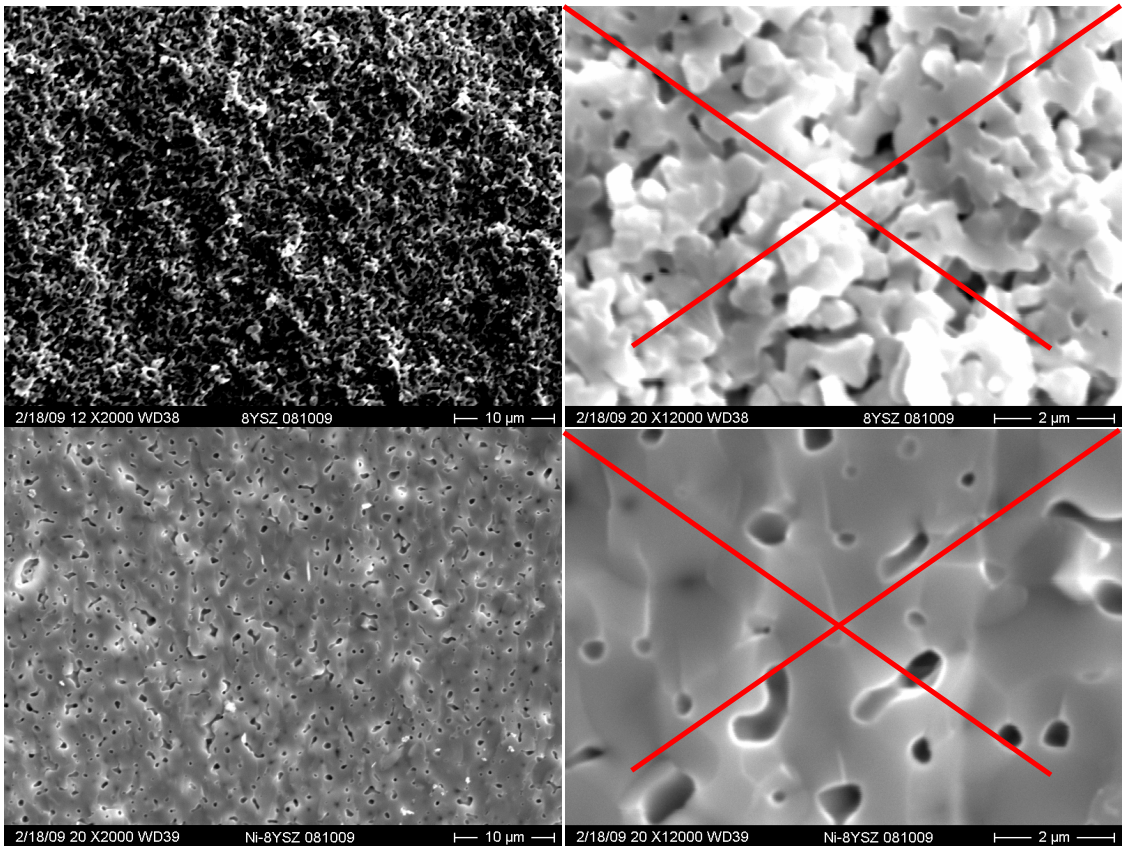

Figure 52. (Top) 8YSZ at 2000x and 12000x. (Bottom) Ni-8YSZ at 2000x and 12000x at 1400C

In the 8YSZ comparison in Figure 52, it is shown that a transgranular fracture occurred with the aid of the nickel powder, creating a smooth surface. The occurrence of

transgranular fracture indicates that the grain boundaries are not the weakest mode of failure, but instead the material powder particle strength is the limiting factor. Ni-3YSZ appears to have a failure across the lattice of the material; conversely, 3YSZ appears jagged and failed mainly at the grain boundaries, as shown in Figure 53.

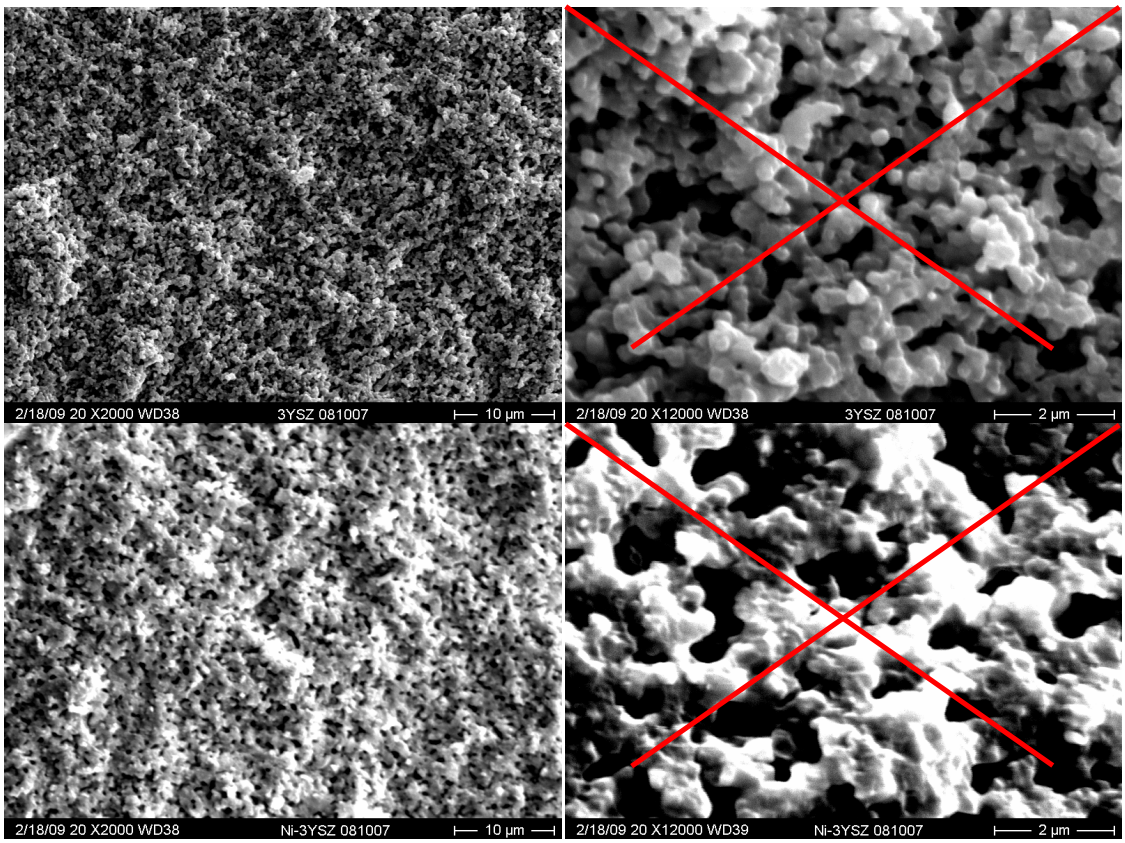

Figure 53. (Top) 3YSZ at 2000x and 12000x. (Bottom) Ni-3YSZ at 2000x and 12000x at 1400C

8YSZ had smaller grain sizes than the nickel doped 8YSZ, while the mode of failure for the 8YSZ was intergranular leaving a rough contour on the fracture surface. Ni-8YSZ appears to have failed transgranularly similar to Ni-8YSZ, creating a smooth surface when sintered at 1300°C. The correlation of the grain size in the 12000x magnification of the 8YSZ and Ni-8YSZ indicates that 8YSZ grain size is 0.35µm and 0.54µm for nickel doped 8YSZ, as seen in Figure 54.

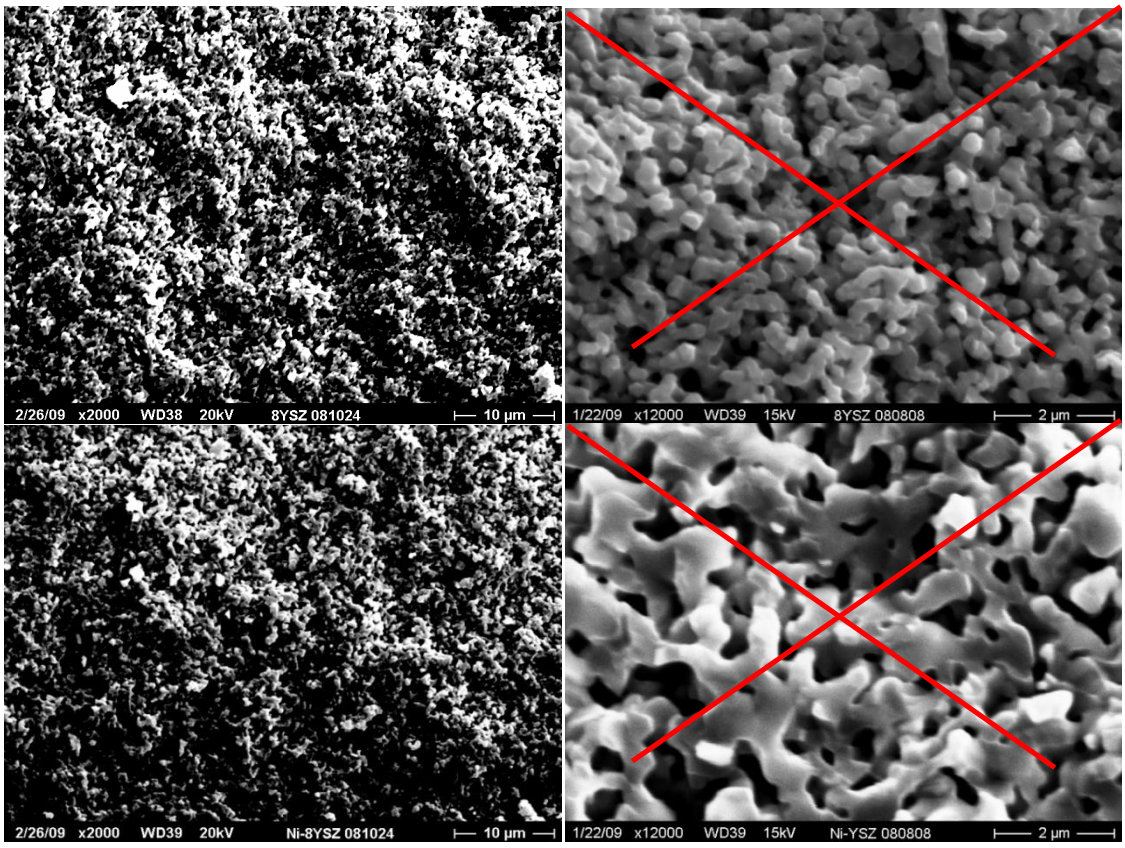

Figure 54. (Top) 8YSZ at 2000x and 12000x. (Bottom) Ni-8YSZ at 2000x and 12000x at 1300C

The 3mol% YSZ has similar surface contours in the low and high magnification as the doped 3mol% YSZ, as shown in Figure 55. Failure occurred at the grain boundaries, resulting in a non-uniform fracture. A comparison of the samples at higher magnification does indicate an increase in the grain size for the nickel doped tape. Grain size for 3mol% electrolyte is 0.41µm while doped 3mol% electrolyte has an average size of 0.52µm.

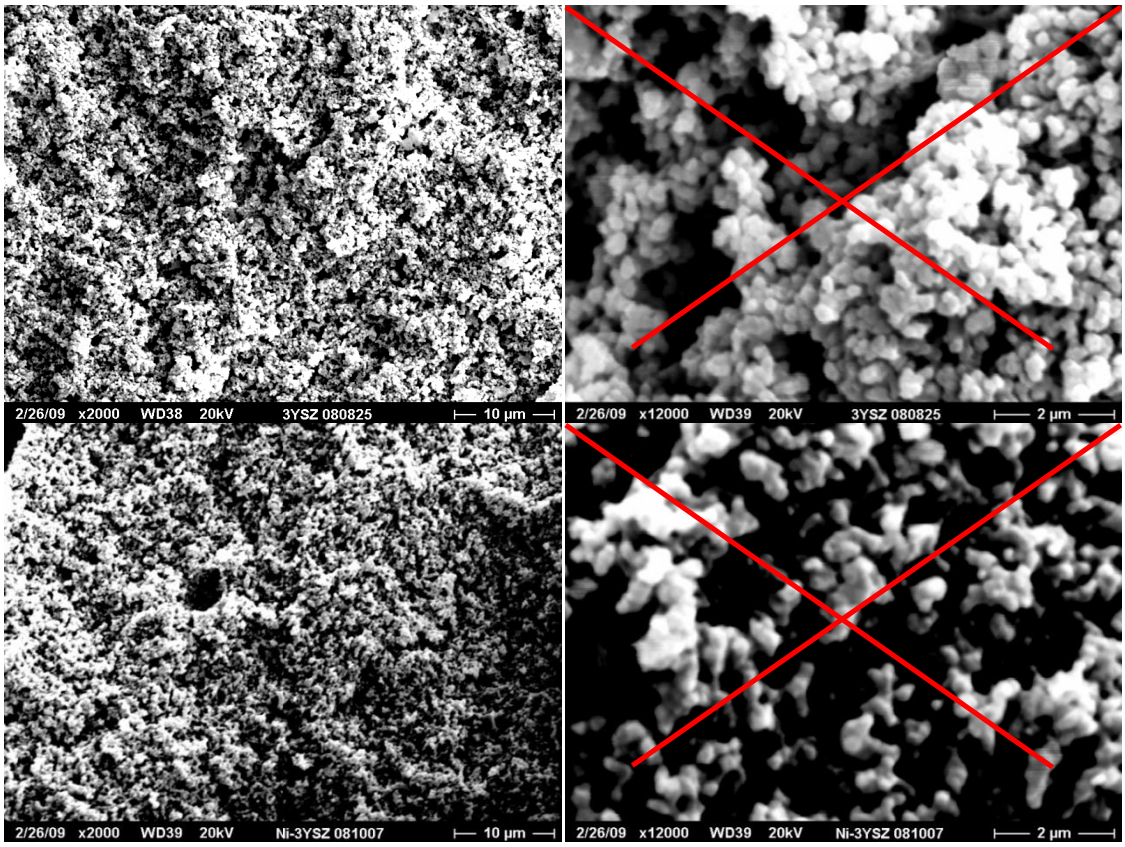

Figure 55. (Top) 3YSZ at 2000x and 12000x. (Bottom) Ni-3YSZ at 2000x and 12000x at 1300C

Nickel oxide doped tapes displayed a different type of mode of fracture with all of the sintering cycles, including the 1250°C, as shown in Figure 56. The nickel doped YSZ fractured smoother with cleaner fracture surfaces when compared to the course fracture surface of YSZ tapes. Fracturing is transgranular when the nickel dopant is present and intergranular with the absence of nickel, leading to speculation that the nickel interacts with the grain boundaries. Grain sizes between the undoped and doped samples of 8YSZ were found to be 0.27µm and 0.34µm, respectively, based on Figure 56.

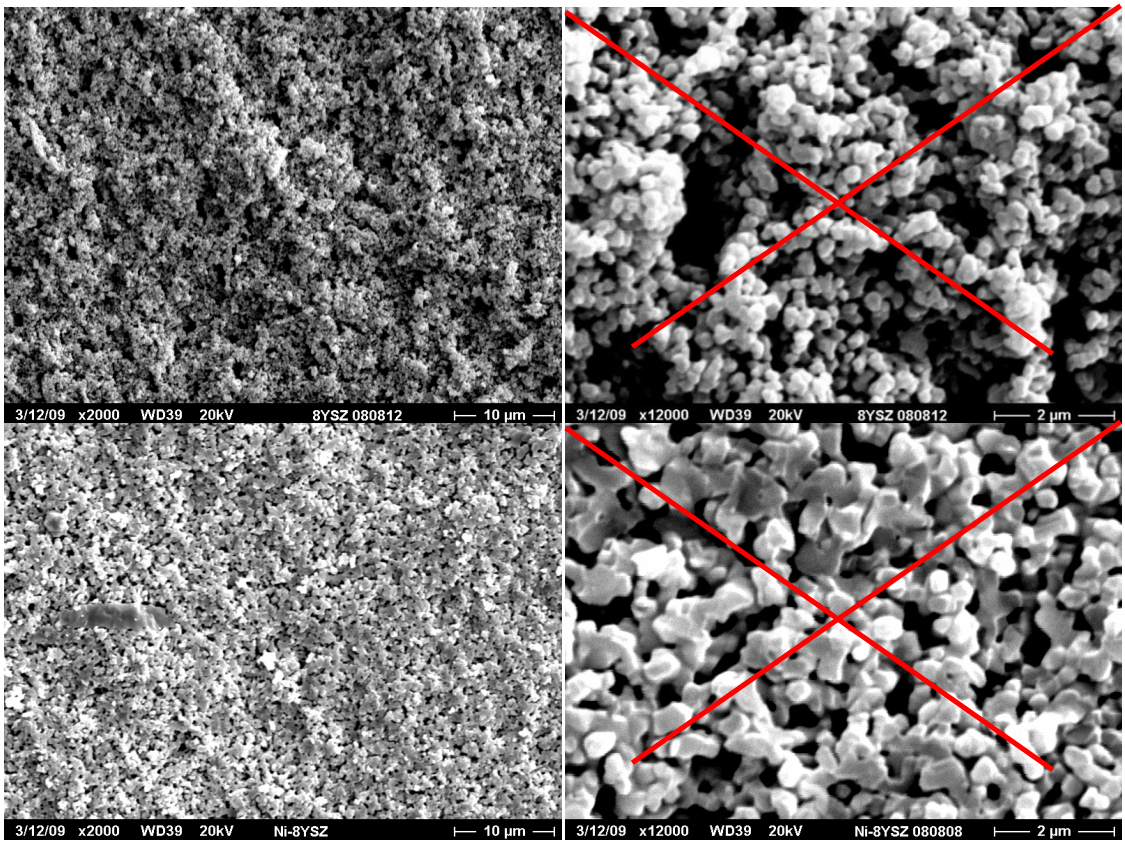

Figure 56. Top 8YSZ at 2000x and 12000x. Bottom Ni-8YSZ at 2000x and 12000x at 1250C

3YSZ doped and undoped samples were compared for those sintered at 1250°C. The last sinter cycle comparison, shown in Figure 57, has similar surface characteristics at a magnification of 2000x. Grain size differs in the two samples at a magnification of 12000x with Ni-3YSZ having a size of 0.44µm and 3YSZ grain size calculated to be 0.31µm. All the grain size averages are shown in Table 9 for doped and undoped samples at each sintering cycle. The data shows an increase for every sintering temperature for the doped samples over the undoped samples. Grains are growing with the addition of the nickel oxide.

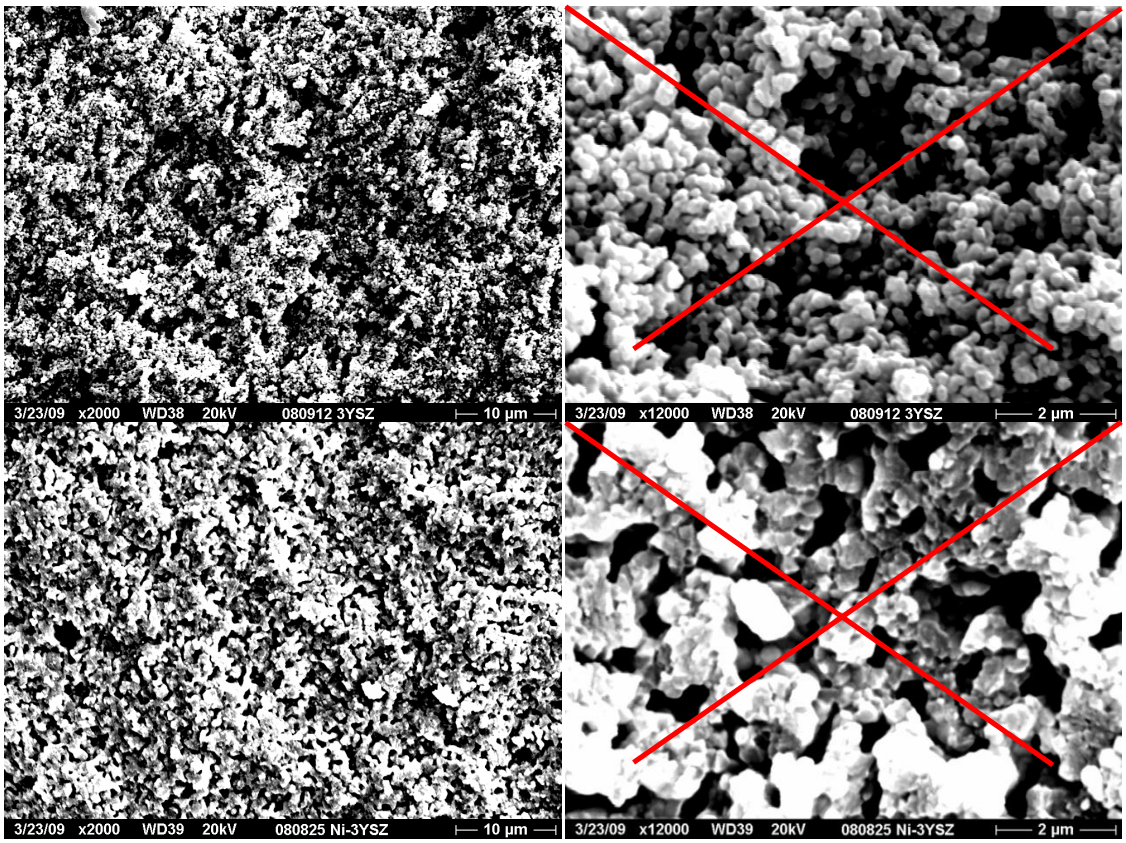

Figure 57. (Top) 3YSZ at 2000x and 12000x. (Bottom) Ni-3YSZ at 2000x and 12000x at 1250C

Table 9. Average Grain Size of Particles for Different Sintering Cycles

Grain Size (µm)				
	8YSZ	Ni-8YSZ	3SYZ	Ni-3YSZ
1400°C	0.74	1.18	0.38	0.61
1300°C	0.35	0.54	0.41	0.52
1250°C	0.27	0.34	0.31	0.44

CONCLUSIONS

Pressed Pellets

Initial density studies of pellets showed that the micro particle size nickel oxide was the optimal choice to test with. The highest percent of theoretical density was achieved with Alfa Aesar nickel oxide. Using micro size powders helped to eliminate particle clustering associated with nano particle powder.

Adding different mole percents of nickel oxide in the range of 0.1, 0.5, and 1 mole % to pellets made from both 3YSZ and 8YSZ improved the sintering performance in every scenario. The highest tested nickel concentration of one mole percent provided the highest post sintering geometric density. This was compared to published values of 1300°C and 1400°C sintering runs that dwelled for one hour. The nickel concentration was limited to 1mol% due to the desired ionic conductivity that electrolyte ceramics require to function. The results indicate that a minimal change occurred between the 0.5 and 1mol% concentration amounts suggesting that additions beyond 1mol% may not yield any advantage.

Dilatometry confirming that the onset sintering temperatures were lower with the doped specimens. Nickel oxide dramatically increased the shrinkage and rate of sintering for the YSZ ceramics. The addition of 1mol% nickel oxide caused the shrinkage of the 8YSZ and 3YSZ to improve by 20.04% and 19.78% respectively. The sintering rate of doped to plain 8YSZ doubled while the rate tripled for 3YSZ. Shrinkage and sintering rate is a function of the amount of nickel oxide additive, showing continued improvement

as concentrations were increased to one mole percent even though the rate of change between 0.5 and 1mol% is minimal.

Ionic conductivity testing of the doped electrolyte membranes indicated that nickel oxide, in trace amounts, had negligible effects when compared to base line electrolyte conductivity. A minor improvement in the grain boundary contribution of the total ionic conductivity was observed with a nickel doped 8YSZ tape sintered at 1300°C for one hour.

Tape Casting

Tape casting densities improved with the addition of nickel oxide dopant. The highest sintered density was achieved with 1 mole % of nickel oxide when using a range of 0.1, 0.5, and 1 mole %. The density of the tape cast parts did not attain densities has high as pressed pellets due to the processing method.

Flexural strength test with ring-on-ring testing indicated increased strength in Ni-YSZ in every tape tested and every sintering process. The average increase of doped samples' strength over the undoped ceramics was approximately 38%. Flaws in the material and manufacturing process in combination with the inherent properties of ceramic material resulted in a range of flexural strength. Strength of the tapes were compared to the chronological order of the tape casting process. The 1400°C sintering process showed a linear increase as the tape casting procedure was refined for both 3YSZ and 8YSZ. The two other sintering stages did not have an increasing slope, but remained consistent.

Density comparisons between YSZ and Ni-YSZ were further illustrated using micrographs obtained from the SEM. With the magnification of 2000x, the surface contour depicts closer packing of the particles, resulting in minimal voids for all sintering cycles. Nickel oxide seems to penetrate and reside in the grain boundaries of the YSZ. 8YSZ and 3YSZ doped samples, under a magnification of 12000x, portrayed a transgranular smooth fracture in each micrograph. Intergranular fracture resulted in jagged edges for the plain YSZ tapes. Grain boundaries were changed by the addition of nickel, apparently increasing the strength in the region causing a transgranular fracture. Grain growth was present in the doped samples suggested enhanced lattice and grain boundary diffusion. Nickel oxide particles were inclusions were not observed in the SEM micrographs suggesting all of the dopant dissolves in the YSZ lattice.

YSZ electrolytes showed a notable increase in density and strength with the addition of trace amounts of nickel oxide dopant. The dopant also enhanced the sintering rate and shrinkage while decreasing the sintering temperature of the ceramic. Ionic conductivity increased with a sintering cycle of 1300°C for one hour. With producing a fully dense electrolyte membrane at a reduced temperature of 1300°C, the feasibility of co-sintering a single cell fuel cell shows merit.

Future Work and Considerations

The data taken for the strength testing contained no outlier data points. Utilizing a Weibull distribution to take into account the outliers a more accurate depiction of flexural than the full data standard deviation. Time constraints limited this

characterization process which can be used in conjunction with the standard deviation. The Weibull distribution could display the trends in the data to determine outlier data points.

Utilizing the four current tape casting recipes and cast a tape of each. Determine optimum grain size, part shrinkage, and density for the 1300°C via thermal gravitametric analysis and dilatometry. Dwell time at the maximum temperature should be determined and ramp rate should also be maximized.

To fully validate the effects of nickel oxide dopants electrochemical tests need to be performed on fully operational cells. A comparison of the power output and degradation between the doped and undoped tape casted electrolyte would provide a comparison of the effects of doped electrolytes. After the test rig, fracture characteristics would be valuable information. Micrographs of the boundaries between the electrodes and the electrolyte would show any migration of nickel from the anode and any possible degradation between the electrolyte and cathode.

A test is underway to examine the effects of Ni diffusion in YSZ. During current co-sintering process a side effect could be the Ni from the anode diffusing into the electrolyte. The co-sintering process might be enhancing the cells properties through diffusion of Ni0 into the electrolyte.

BIBLIOGRAPHY

1. *Ionic conductivity of plasma-sprayed nanocrystalline yttria-stabilized zirconia electrolyte for solid oxide fuel cells.* Chen, Y.1, et al. 11, s.l. : Elsevier Ltd, 2002, Vol. 60.

2. *Interface reactions during co-firing of solid oxide fuel cell components* . Rajendra N. Basu, Frank Tietz , Egbert Wessel and Detlev Stöver. 1, s.l. : Elsevier B.V., 2003, Vol. 147.

3. *Reaction kinetics and mechanisms between La0.65Sr0.3MnO3 and 8 mol% yttria-stabilized zirconia.* Yang, Chih-Chung T.1, Wei, Wen-Cheng J.1 and Roosen, Andreas2. 6, s.l. : American Ceramic Society, 2004, Vol. 87.

4. Fuel Cell. *Answers.com.* [Online] Answers Corporation, 2009. [Cited: 03 24, 2009.] http://www.answers.com/topic/fuel-cell.

5. Guire, Eileen J. De. Solid Oxide Fuel Cells. *Pro Quest.* [Online] April 2003. [Cited: November 7, 2008.] http://www.csa.com/discoveryguides/fuecel/overview.php?SID=hoe502octckfqhg36n3b5park1.

6. Young, J.B. Gibbs and Nernst Potential of SOFCs. *http://www.fuelcellknowledge.org/.* [Online] 09 09, 2003. [Cited: 05 7, 2009.] http://www.fuelcellknowledge.org/research_and_analysis/cell_performance/gibbs_nernst_potential/gibbs_nernst_potential.pdf.

7. *Fuel Cell Materials and Components.* Haile, Sonnina M. s.l. : Elsevier Ltd, 08 31, 2003, Scinence Direct, Vol. 51, p. 20.

8. Sofie, Dr. Stephen. *Overall Reaction.* Montana State Univeristy, Bozeman : 2008.

9. Energy, US Department of. Fuel Cell Handbook (Seventh Edition). Morgantown, West Virgina : US Department of Energy, November 2004.

10. *Cation transport behavior in SOFC cathode materials of La0.8Sr0.2CoO3 and La0.8Sr0.2FeO3 with perovskite structure* . Haruo Kishimoto, a, , Natsuko Sakaia, Teruhisa Horitaa, Katsuhiko Yamajia, Manuel E. Britoa and Harumi Yokokawaa. 21-22, s.l. : Elsevier B.V., 2007, Vol. 178.

11. *Development of lanthanum ferrite SOFC cathodes* . S. P. Simner, , J. F. Bonnett, N. L. Canfield, K. D. Meinhardt, J. P. Shelton, V. L. Sprenkle and J. W. Stevenson. 1, s.l. : Elsevier Science B.V., 2002, Vol. 133.

12. *Fabrication of Dense Zirconia Electrolyte Films for.* B.V., Elsevier Science. 1, s.l. : American Ceramic Society, 2001, Vol. 84.

13. Garrison, Earnest. Fuel Cell Basics . *Solid Oxide Fuel Cells.* [Online] 07 16, 2006. [Cited: 05 10, 2009.] http://www.iit.edu/~smart/garrear/fuelcells.htm.

14. Fuel Cell Basics How They Work. *Fuel Cells 2000.* [Online] [Cited: November 22, 2008.] www.fuelcells.org/basics/how.html.

15. Yittria Stabilized Zirconia (8 Mol. %). *American Elements.* [Online] 2001-2009. [Cited: 03 24, 2009.] http://www.americanelements.com/ysz.html.

16. *Yttria Stabilized Zirconia (8 Mol. %).* [Online] American Elements, 2009. [Cited: 05 10, 2009.] http://www.americanelements.com/ysz.html.

17. *Geometrical modeling of the triple-phase-boundary in solid oxide fuel cells* . Xiaohua Deng, and Anthony Petric. 2, s.l. : Elsevier B.V. , 2004, Vol. 140.

18. *A symmetrical, planar SOFC design for NASA's high specific power density requirements* . Thomas L. Cablea, , and Stephen W. Sofieb, 1. 1, s.l. : Elsevier B.V. , 2007, Vol. 174.

19. Yanhai Du*, Nigel M. Sammes, Ray England. Novel SOFC Tubular Design Configurations. [Online] Connecticut Global Fuel Cell Center. [Cited: 05 10, 2009.] http://www.electrochem.org/dl/ma/203/pdfs/1921.pdf.

20. Singhal, Subhash C. SOLID OXIDE FUEL CELLS . *Electrochemistry Encyclopedia.* [Online] Pacific Northwest National Laboratory, 03 2008. [Cited: 05 10, 2009.] http://electrochem.cwru.edu/encycl/art-f02-sofc.htm.

21. The Tubular Design. *Siemens.* [Online] 2007. [Cited: 03 25, 2009.] www.powergeneration.siemens.com.

22. Planar SOFC. *SOFC.* [Online] 2008. [Cited: 03 25, 2009.] http://kunisan.jp/gomi/sofc.html.

23. SOFC / Gas Turbine Hybrid. *Siemens* . [Online] 2007. [Cited: 03 26, 2009.] www.powergeneration.siemens.com/products-solutions-services/products-packages/fuel-cells/sofc-gt-hybrid/.

24. Nasr, Susan. More Powerful Fuel Cells Get Closer To Market. *Technology Review.* [Online] MIT, 06 13, 2006. [Cited: 05 10, 2009.] http://www.technologyreview.com/read_article.aspx?id=16965&pg=1.

25. *Solid oxide fuel cell micro combined heat and power system operating strategy: Options for provision of residential space and water heating* . A.D. Hawkesa, , , P. Aguiarb, B. Croxfordc, M.A. Leacha, C.S. Adjimanb, d and N.P. Brandon. 1, s.l. : Elsevier B.V, 2006, Vol. 164.

26. Sofie, Dr. Stephen. *Hybridized SOFC.* Bozeman : 2006.

27. *Regenerative Adsorption and Removal of H2S from Hot Fuel Gas Streams by Rare Earth Oxides* . Maria Flytzani-Stephanopoulos, * Mann Sakbodin, Zheng Wang. 5779, s.l. : Science, 2006, Vol. 312.

28. Husain, Iqbal. Alternative Energy Sources. *Electrci and Hybrid Vehicles Design Fundamentals.* s.l. : CRC Press, 2003.

29. *SOFC-type microreactors that generate hydrogen for PEFC applications.* Atsuko Tomitaa, Daisuke Hirabayashia, Masahiro Nagaob, Mitsuru Sanob and Takashi Hibinob. 1-4, s.l. : Elsevier Ltd, 09 11, 2004, Vol. 174.

30. What are Ceramics? *MAST Materials Science and Technology* . [Online] [Cited: January 13, 2009.] http://matse1.mse.uiuc.edu/ceramics/ware.html.

31. About Oxide Ceramics (Alumina, Zirconia, Silicates). *Global Spec An Engineering Search Engine.* [Online] GlobalSpec, 2009. [Cited: 1 14, 2009.] http://materials.globalspec.com/LearnMore/Materials_Chemicals_Adhesives/Ceramics_Glass_Materials/Oxide_Ceramics_Alumina_Zirconia_Silicates.

32. Vlack, Lawrence H. Van. *Physical Ceramaics For Engineers.* USA : Addison-Wesly Publishing Company, INC., 1964.

33. *Advanced Ceramics – The Evolution, Classification, Properties, Production, Firing, Finishing and Design of Advanced Ceramics.* Taylor, D.A. 1, s.l. : Materials Australia, 2009, Vol. 33.

34. *Ceramic sensors for humidity detection: The state-of-the-art and future developments* . Traversa, E. 2-3, s.l. : Elsevier Science, 1995, Vol. 23.

35. *Materials issues in design and performance of piezoelectric actuators: an overview* . Uchino, K.a. 11, s.l. : Elsevier Science , 1998, Vol. 46.

36. ceramic composition and properties. *Encyclopedia Britannica.* [Online] ceramic composition and properties, 2009. [Cited: 05 10, 2009.] <http://www.britannica.com/EBchecked/topic/1359519/composition-and-properties-of-ceramics>. .

37. Joseph E. Shigley, Charles R. Mischke, & Richard G. Budynas. *Mechanical Engineering Design, 7th ed.* New York : McGraw-Hill, 2004.

38. Lorentz number. *answers.com.* [Online] Answers Corporation, 2009. [Cited: 05 10, 2009.] http://www.answers.com/topic/lorentz-number.

39. *Relaxation Model for Heat Conduction in Metals.* Maurer, Michael J. 5123, New Orleans : The American Institute of Physics , 1970, Vol. 40.

40. D. Munz, T. Fett. *Ceramics Mechanical Properties, Faliure Behaviour, Materials Selection.* New York : Springer-Verlag New York, LLC, 2001. 3540653767.

41. NDT. *Electrical Conductivity and Resistivity.* [Online] 2009. [Cited: 05 10, 2009.] http://www.ndt-ed.org/EducationResources/CommunityCollege/Materials/Physical_Chemical/Electrical.htm.

42. Mistler, Richard E. and Twiname, Eric R. *Tape Casting Theory and Practice.* Westerville, Ohio : The American Ceramic Society, 2000.

43. Sintering of Ceramics. *SubsTech.* [Online] 02 05, 2008. [Cited: 1 28, 2009.] http://www.substech.com/dokuwiki/doku.php?id=sintering_of_ceramics.

44. *Sinterability of Agglomerated Powders.* LANGE, F. F. 2, Thousand Oaks : American Ceramic Society, 2006, Vol. 67.

45. *Binary solvent mixture for tape casting of TiO2 sheets* . Zhang Jingxian, Jiang Donglianga, Lars Weisenselb and Peter Greilb. 1, s.l. : Elsevier Ltd., 2004, Vol. 24.

46. Clark, Jim. INTERMOLECULAR BONDING - VAN DER WAALS FORCES. [Online] 200. [Cited: 05 10, 2009.] http://www.chemguide.co.uk/atoms/bonding/vdw.html.

47. Kostadin Petkov, Mark Wesselmann. A Practical Aqueous Tape Casting Binder. *Ceramic Industry.* [Online] Polymer Innovations, Inc., 05 01, 2007. [Cited: 05 10, 2009.] http://www.ceramicindustry.com/Articles/Feature_Article/BNP_GUID_9-5-2006_A_10000000000000099143.

48. Joanna R. Groza, James F. Shackelford, Enrique J. Lavernia, Michael T. Powers. *Materials Processing Handbook.* Boza Raton : Taylor and Francis Group, LLC, 2007.

49. Processing Sintering or Firring. *Dynamic Ceramic Percision Engineering Ceramic Solutions.* [Online] DYNAMIC-CERAMIC LTD , 2008. [Cited: 1 28, 2009.] http://www.dynacer.com/sintering.htm.

50. Generalic, Eni. *Chemistry Dictionary and Glossary.* [Online] 2005. [Cited: 1 29, 2009.] http://www.ktf-split.hr/glossary/no_en_o.php?def=ball%20mill.

51. THINKY Technology. *THINKY.* [Online] [Cited: 1 29, 2009.] http://thinkyusa.com/performance.aspx.

52. Kopeliovich, Dmitri. Methods of shape forming ceramic powders. *SubsTech.* [Online] 02 05, 2008. [Cited: 01 29, 2009.] http://www.substech.com/dokuwiki/doku.php?id=methods_of_shape_forming_ceramic_powders.

53. Doctor Blading. *Encyclopædia Britannica.* [Online] 2009. [Cited: 02 03, 2009.] http://www.britannica.com/EBchecked/topic/167379/doctor-blading .

54. *Effect of nanopowder deagglomeration on the densities of nanocrystalline ceramic green bodies and their sintering behaviou.* Hellmiga, H. Ferkela and R. J. 5, s.l. : Elsevier Ltd, 01 20, 1999, Vol. 11.

55. *Impedance spectroscopy of YSZ electrolyte containing CuO for various applications.* M. El-sayed Alia, Omar A. Abdelala and Ahmed A. Hassan. 25-26, s.l. : Elsevier Ltd, 09 21, 2007, Vol. 178.

56. Scanning Electron Microscope. *Radiological and Envionmental Management.* [Online] 10 06, 2006. [Cited: 03 18, 2009.] http://www.purdue.edu/REM/rs/sem.htm.

57. Scanning Electron Microscope (SEM). *Imaging and Chemical Analysis Laboratory.* [Online] [Cited: 03 18, 2009.] http://www.physics.montana.edu/ical/instrumentation/sem.asp.

58. Introduction to Thermomechanical Analysis . *Anasys Thermal Methods Consultancy.* [Online] [Cited: 03 18, 2009.] http://www.anasys.co.uk/library/tma1.htm.

59. Evgenij Barsoukov, J. Ross Macdonald. *Impedance Spectroscopy Theory, Experiment, and Applications Second Edition.* New Jersey : John Wiley and Sons, Inc., 2005. 0-471-64749-7.

60. Mark E. Orazem, Bernard Tribollet. *Electrochemical Impedance Spectroscopy.* New Jersey : John Wiley and Sons, Inc., 2008. 978-0-470-04140-6.

61. Standard Test Method for Monotonic Equibiaxial Flexural Strength of Advanced Ceramics and Ambient Temperture. *ASTM International.* s.l. : Annual Book of ASTM Standards, 2006. Vol. 15.01.

62. *NIST Structural Ceramics Database (SCD).* [Online] [Cited: 04 16, 2009.] http://www.ceramics.nist.gov/srd/scd/Z00268.htm#M7P6.

63. M. Ghateea, M.H. Shariata and J.T.S. Irvineb. Investigation of electrical and mechanical properties of 3YSZ/8YSZ composite electrolytes . *Science Direct.* [Online] Elsevier B.V., 12 04, 2008. [Cited: 04 16, 2009.] http://www.sciencedirect.com/science.

64. Gentile, Paul S. *Development of a Novel High Performance Electrolyte Supported.* Bozeman : Montana State University, 2007.